Light-Induced Redox Reactions in Nanocrystalline Systems

Anders Hagfeldt† and Michael Grätzel*

Institut of Physical Chemistry, Swiss Federal Institute of Technology, CH-1015 Lausanne, Switzerland

Received June 9, 1994 (Revised Manuscript Received August 8, 1994)

Contents

1. Introduction

This review discusses salient features of interfacial electron transfer reactions in colloidal semiconductor solutions and thin films and their application for solar light energy conversion and photocatalytic water purification.[1] This research is interdisciplinary and is situated at the limit between colloid science, electrochemistry, and semiconductor physics. Several intriguing features arise from the symbiosis of these areas of research. Colloidal science teaches us how to prepare very small semiconductor particles and how to stabilize these aggregates with respect to coagulation. Furthermore, it provides useful information on the surface thermodynamics of the colloid, e.g. electrostatic potential, acid base properties of surface hydroxyl groups, specific adsorption, electrolytic double layer properties, electrophoretic properties, etc. The electronic properties of the particles, on the other hand, relate to their solid state physics aspects, i.e. band structures and band gap, charge carrier mobilities and lifetimes, as well as the electrochemical positioning of the band edge potential with respect to the Nernst potential of the solution. Of particular importance are further quantum effects which arise when the size of the semiconductor particles becomes smaller than the Bohr radius of the first exciton state. Numerous important properties of the semiconductor, such as its optical absorption and luminescence emission, undergo drastic changes in this size domain.

A newly emerging research front which has given great impetus to the studies on colloidal semiconductors is that of heterogeneous photocatalysis. The size of the colloidal particles is generally small enough to render their solutions optically transparent allowing for convenient analysis of the elementary steps involved in the catalytic process. The use of time-resolved techniques such as laser photolysis will be described to derive the rate constant for electron–hole recombination within the TiO_2 particles and within nanocrystalline TiO_2 films of very high internal surface area. This technique has allowed the identification of the factors that govern the dynamics of interfacial electron and hole transfer reactions. Thus, the photocatalytic destruction of carbonaceous environmental pollutants in aqueous solutions comprises oxidation of the organic compound by valence band holes and this is coupled to the reduction of oxygen by conduction band electrons. Since the latter process occurs at a slow rate, it is often rate determining.[2] Therefore, to increase the efficiency of the TiO_2 photocatalysts, means have to be found to increase the rate of oxygen reduction. Judicious surface modification of the TiO_2, e.g. by chelating groups, was found to lead to a drastic acceleration of this important conduction band process.[3] Recent and very active research relates to the anchoring of charge transfer dyes to wide band gap semiconducting colloids rendering them sensitive to visible light.[4] Heterogeneous catalysts are frequently deposited onto the surface of the semiconductor to enhance multielectron transfer reactions such as the oxidation and reduction of water and this has received a great

* Author to whom correspondence should be addressed.
† Present address: Department of Physical Chemistry, Box 532, S- 751 21 Uppsala, Sweden.

0009-2665/95/0795-0049$15.50/0

Anders Hagfeldt was born in Norrköping, Sweden, on February 16, 1964. He received a M.Sc. (1989) and a Ph.D. (1993) in physical chemistry from the University of Uppsala, under the guidance of Dr. Sten-Eric Lindquist and Dr. Hans Seigbahn. His thesis concerned nanocrystalline TiO_2 electrodes and small semiconductor particles, investigated by, for example, photoelectron spectroscopy and quantum chemical calculations. At present he is a postdoctoral fellow with Professor Michael Grätzel at EPFL in Lausanne, Switzerland. His present research activities are studies on the charge carrier separation and transport in nanocrystalline TiO_2 films and development of these systems for electrochromism and electrocatalysis. He is married (Camelia) with two children (Mikael and Rebecka).

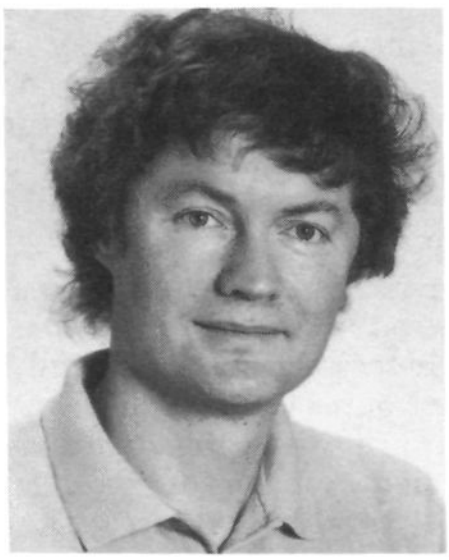

Since 1977, Michael Grätzel has been a Professor at the Institute of Physical Chemistry at the Swiss Federal Institute of Technology in Lausanne, Switzerland. He served as Head of the Chemistry Department from 1983 to 1985 and from 1991 to 1993. His laboratory has been active in developing functional micelles and artificial membrane assemblies which are used to mimic the primary events of photosynthesis. It pioneered studies in the domain of colloidal semiconductor particles and nanocrystalline semiconductor films. These systems are applied in a variety of fields, such as highly efficient light harvesting devices and biosensors. Recently, a new type of solar cell was developed based on nano-structured colloidal semiconductor films. Professor Grätzel, who is the author of over 400 publications, two books, and 10 patents, regularly performs research as a guest scientist at foreign laboratories. He has been invited as a Visiting Professor at the University of California at Berkeley and the Lawrence Berkeley Laboratory and has held honorary lectureships from the British Council and the University of Texas at Austin and was awarded a fellowship of the Japanese Society for the Promotion of Science. He is a member of several editorial boards and acts a consultant to international industrial corporations.

deal of attention in context with ongoing studies on the photocleavage of water. This review focuses on the factors that govern electron transfer reactions in colloidal semiconductor assemblies. In addition we shall discuss electronic processes in nanocrystalline films that constitute an exciting new area of research in heterogeneous photochemistry.

2. Colloidal Semiconductors

2.1. Material Science Aspects

Colloids are commonly distinguished from macroparticles by their size. The latter have a radius exceeding 1000 Å and form turbid suspensions. Colloids are smaller particles and give clear solutions. Semiconductors with colloidal dimensions have been prepared from many materials and it has been more than a decade ago since we published the first accounts on light driven redox reactions with such nanocrystalline systems.[5-7] Since then there has been an explosion of information in this field which has been the subject of many reviews.[8-18] Particularly well studied have been oxides and sulfides or selenides, e.g. TiO_2,[19] ZnO,[20] WO_3,[21] V_2O_5,[22] Ag_2O,[23] ZnS,[24] CdS,[25] PbS,[26] Cu_2S,[27] MoS_2,[28] and CdSe.[29] Other materials such as Cd_3P_2[30] or HgI_2[31] display intriguing quantum size effects in their absorption and luminescence properties and have been investigated mainly for this reason. The preparation often involves chemical methods. The semiconductor material is precipitated from solutions containing suitable precursors. Care must be taken to arrest the precipitation before formation of large agglomerates has occurred. This is usually done by carrying out the synthesis in the presence of a suitable protective agent. A wide variety of semiconductor particles has been prepared in this way in solutions,[32-39] glasses,[40,41] and polymers[42,43] although their identification is sometimes not unambiguous.[44]

Alternative methods of synthesizing colloidal semiconductor aggregates employ the use of solid matrices such as porous glasses[45] or zeolites.[46] The size and shape of the semiconductor is determined in this case by the morphology and texture of the microscopic voids of the host template where aggregation occurs. For example, a novel class of semiconductor/zeolite composite materials has been prepared where well-defined $(CdS)_4$ clusters are stabilized inside the 5 Å sodalite cages of a zeolite.[47] The tetramers are interconnected forming an extended structure, referred to as superclusters. These materials can be viewed as three-dimensional arrays of mutually interacting quantum dots with geometric structures imposed by the zeolites' internal pore structure. Different spatial arrangements of these quantum dots can be achieved by using zeolites as templates.

Other ways to achieve size control in the chemical precipitation of semiconductor colloids involve organized molecular assemblies, such as inverted micelles and vesicles.[48,49] Arrested precipitation in these structured media has been combined with chemical modification of the surface for nanometer-sized CdSe clusters using an organometallic reagent and AOT inverted micelles.[50] The formation of colloidal semiconductors in monolayer films has also been recently achieved.[51] Finally, it is noteworthy that the mere dissolution of a powder in an organic solvent assisted by sonication can give rise to the formation of very small semiconductor aggregates. For example, Peterson et al. have obtained quantized (10 − 35 Å-sized) particles of MoS_2 and WS_2[28] by this method in acetonitrile. Since both materials have a layered structure, it was suggested that the clusters are

formed by cleavage of the van der Waals layers by penetrating solvent molecules. A similar process is known to occur during the colloidal formation from layered clay structures. X-ray analysis has shown in all these cases that even very small semiconductor particles can be produced with a high degree of crystallinity.

Colloidal semiconductors may be used as building blocks to form assemblies with new solid sate properties. For example, CdS clusters incorporated into zeolites are interconnected through the sodalite channels within the porous network of the host yielding a "supercluster". Similarly, nanometer-sized particles of TiO_2 can be assembled to thin transparent films whose inner surface area is enormous.[53,54] The colloidal particles forming the assembly are in electronic contact allowing for electric charge percolation through such films. We shall discuss further below the use of such films for the optical measurement of the flat band potential of the colloidal particles and their application for the development of a new type of photovoltaic device.

2.2. Optical Properties

2.2.1. Optical Absorption of Colloidal Semiconductor Particles, Mie Theory

Semiconductors absorb light below a threshold wavelength λ_g, the fundamental absorption edge, which is related to the band gap energy via[55]

$$\lambda_g\,(\mathrm{nm}) = 1240/E_g\,(\mathrm{eV}) \tag{1}$$

Within the semiconductor, the extinction of light follows the exponential law:

$$I = I_0 \exp(-\alpha l) \tag{2}$$

where l is the penetration distance of the light and α the reciprocal absorption length. For example, for TiO_2 α has the value 2.6×10^4 cm^{-1} at 320 nm which implies that light of wavelength 320 nm is extinguished to 90% after traversing a distance of 3900 Å.

Near threshold, the value of α increases with increasing photon energy. Frequently a function of the type

$$\alpha h\nu = \mathrm{const}\,(h\nu - E_g)^n \tag{3}$$

gives a satisfactory description of the absorption behavior in this wavelength domain. Here, the exponent has the value 0.5 for a direct transition and 2 for an indirect one.[55] A direct transition is characterized by the fact that in the electronic energy vs wave vector diagram, the minimum in the conduction band states is placed vertically above the maximum in the valence band energy states (Figure 1a). By contrast, for an indirect transition the two extremes are displaced from each other. As a consequence, the threshold excitation requires a contribution of lattice phonons in order to compensate for the change in the wave vector during the transition (Figure 1b). This reduces the absorption cross section and hence the value of α.

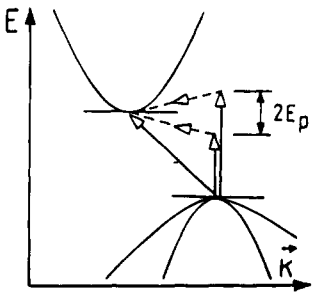

Figure 1. Energy vs wave vector diagram illustrating the band structure for a semiconductor with an indirect gap. E_p is the contribution of lattice vibrations to the transition energy.

In some cases, deviations from eq 3 have been observed. For example, Dutton[56] found that for CdS, the reciprocal absorption length near band edge showed an exponential dependence on photon energy:

$$\ln \alpha = \beta h\nu/kT \tag{4}$$

The coefficient β had a value of 2.1 for single crystals with hexagonal structure colloidal particles yielding significantly smaller values.[57]

In solution, colloidal semiconductor particles remove light from the incident beam both by scattering and absorption. In the absence of quantum size effects the extinction spectrum is described by the Mie theory.[58] Mie obtained a rigorous solution of absorption and scattering by a single sphere. This can be applied to a collection of spheres if a number of conditions are satisfied.[59] Thus, the distance between spheres must be larger than the wavelength so that the spheres scatter independently and the spheres must be randomly oriented. If, in addition, the particles are much smaller than the incident light ($R \ll \lambda$) one obtains for the reciprocal absorption length (unit cm^{-1}) of the light in a solution containing the colloid:

$$\alpha = \frac{18\pi c_p V_p n_s{}^3 \epsilon_2}{\lambda(\epsilon_1 + n_s{}^2)^2 + \epsilon_2{}^2} \tag{5}$$

where $\epsilon = \epsilon_1 + i\epsilon_2$ is the complex dielectric constant of the particle, c is the particle concentration, expressed in number of particles per unit volume, V_p is the volume of one particle, n_s is the refractive index of the solvent in which the colloid is dispersed, and λ is the wavelength of the incident light.

The significance of the dielectric constants ϵ_1 and ϵ_2 becomes clearer by expressing ϵ in terms of the complex refractive index of the particle

$$\epsilon = (n_p + ik_p)^2 = n_p{}^2 - k_p{}^2 + i(2k_p n_p) \tag{6}$$

where n_p is the real refractive index of the particle and k_p is the absorption index which is proportional to the reciprocal absorption length α_p within the particle for light with wavelength λ

$$k_p = \alpha_p \lambda/4\pi \tag{7}$$

Thus, ϵ_1 is identified with $n_p{}^2 - k_p{}^2$ and ϵ_2 with $2n_p k_p$. Therefore, the imaginary part of the dielectric constant is a direct measure of the light absorption by

the particles. It increases steeply near the fundamental absorption edge.

Mie's theory has been widely applied to interpret the extinction spectra of colloidal dispersions, in particular metal sols.[59] For example, the brilliant ruby colors of colloidal golds as well as the yellow color of colloidal silver are well explained by this electromagnetic theory. The advent of experimental techniques to prepare monodispersed sols has allowed the study of the effect of particle size on the extinction spectra. In this regard, a recent investigation by Hsu and Matievic on colloidal α-Fe_2O_3, a semiconductor with a band gap of 2.2eV, is noteworthy.[60] Within the 0.1−0.16 nm size range, the optical spectra of these hydrosols agreed well with the predictions of the Mie theory.

2.2.2. Optical Absorption of Very Small Particles, Quantum Size Effects

At very small particle radii, deviations from the Mie equation occur and this is due to the size quantization effects which were alluded to earlier on. Size quantization effects have been widely investigated in the past for metal particles.[61,62] Effects arising from the spatial confinement of charge carriers in semiconductors have also been the subject of intensive investigations.[63,64] There is much current effort to fabricate materials where excitons are confined in two and three dimensions, often referred to as quantum wires and quantum dots, respectively. Small colloidal semiconductors belong to the latter category. Earlier observations of confinement effects in these systems concerned small CdS particles in glass matrices[65,66] which show blue-shifted absorption and emission spectra. Systematic investigations of quantum size effects in small semiconductor particles date back to the pioneering work of Berry[67] on silver halide microcrystals. Quantum size effects are expected to occur when the Bohr radius of the first exciton in the semiconductor becomes commensurate with or larger than that of the particle. The Bohr radius

$$r_B = h^2\epsilon_0\epsilon/(e^2\pi m^{eff}) \quad (8)$$

depends on the dielectric constant and the effective mass of the charge carrier (m^{eff}). For example, in the case of CdS, $\epsilon = 8.9$ and $m_{e^-}^{eff} = 0.2\ m_{e^-}$ yielding for the Bohr radius of the electron 24 Å. Given the ease of preparation of such small CdS particles it is not surprising that much of the earlier studies on quantum size effects in colloidal semiconductors has been carried out with this material. Particularly noteworthy is the work of Papavassiliou (for a review cf. ref 59) and Hayashi et al.[68] who discovered a blue shift in the absorption and luminescence emission of small CdS particles when their radius decreased below the size where charge carrier confinement effects should become noticeable. Similar observations were made by Stasenko[69] and Skomyakov et al.[70] in their research concerning quantum size effects in CdS microcrystals.

Apart from increasing the effective band gap, the effect of local confinement of the charge carriers is to produce discrete electronic states in the valence and conduction bands. The latter effect is analogous to size quantization observed in small metal particles. To a first approximation, the energy spacing between quantized levels is inversely proportional to the effective mass and the square of the particle diameter. A schematic illustration of these confinement effects is given in Figure 2.

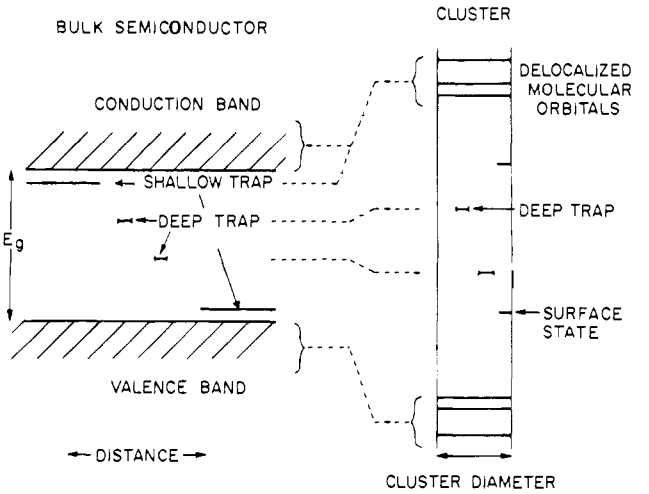

Figure 2. Spatial electronic state correlation diagram for bulk semiconductors and clusters. (Adapted from ref 33.)

The consequences of size quantization for the absorption features of a semiconductor dispersion can be quite dramatic. Thus, HgSe colloids consisting of large particles (500 Å) are black since the band gap of the bulk material is only 0.3 eV corresponding to an absorption threshold at 4130 nm. Due to the very low effective electron mass $^*m_{e^-} = 0.05m_{e^-}$, the band gap of HgSe is strongly dependent on particle size. For example, the absorption threshold for 30 Å-sized particles is at 380 nm implying that the band gap of the semiconductor has increased to 3.2 eV.[71] Similar effects have been observed with other materials, such as PbSe,[26] Cd_3As_2,[30] ZnO,[20] and Zn_3P_2.[72]

Several attempts have been made to calculate the electronic energy levels in such quantum dots. According to Brus,[73] the energy of the first excitonic state of a semiconductor cluster with radius R is given by the approximate expression:

$$E_g(R) = E_g(R=\infty) + \frac{h^2\pi^2}{2R^2}\left[\frac{1}{m_{e^-}} + \frac{1}{m_{h^-}}\right] - \frac{1.8e^2}{\epsilon R} \quad (9)$$

The first term in this equation is the band gap of the bulk semiconductor, the second term corresponds to the sum of the confinement energies for the electron and the hole and the last is their Coulomb interaction energy.

The Coulomb term shifts $E(R)$ to smaller energy as R, while the quantum localization terms shift $E(R)$ to higher energy as R^2. As a result, the apparent band gap will always increase for small enough R. Calculations with more refined quantum mechanical models have recently been carried out.[74,75]

2.2.3. Quantum Size Effects in the Photoluminescence of Colloidal Semiconductors

Due to the quantum effects discussed above, the luminescence of colloidal semiconductors, similar to

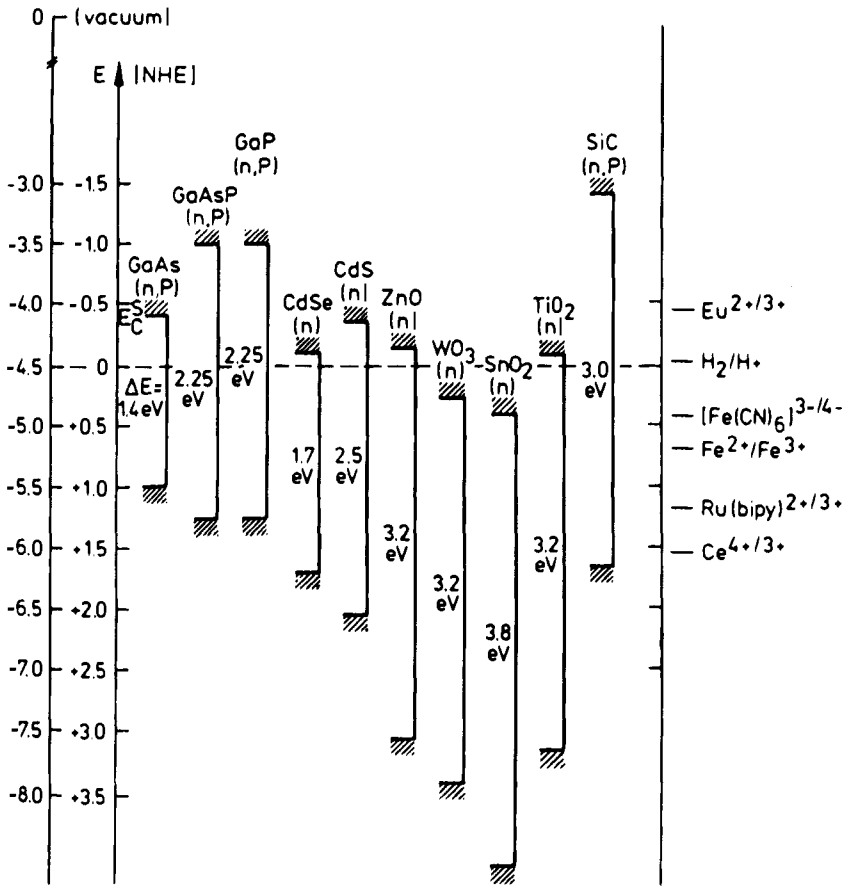

Figure 3. Band edge position of several semiconductors in contact with aqueous electrolyte at pH 1.

the band edge absorption, is strongly influenced by the particle size. Typically, a broad emission is observed which blue shifts with decreasing radius of the aggregate. Effects of this type were first analyzed by Papavassiliou on extremely small CdS particles[59] and have been confirmed in the work of Brus,[73] Henglein et al.,[20,30,71] Nozik et al.,[69] Herron et al.,[47] and our own studies.[57] The luminescence of these clusters is readily detectable at 298 K and can be quite strong at cryogenic temperatures.

Luminescence analysis provides an important tool to study the dynamics of charge carrier recombination in such colloidal semiconductors. For CdS clusters in alcohol glasses, the emission decay time is wavelength and temperature dependent, but it becomes temperature independent below 30 K.[74] In this temperature range, the reciprocal luminescence lifetime, $1/\tau$, for 22 Å-sized clusters is 10^5 s^{-1} and 4.5×10^4 s^{-1} at 580 and 400 nm, respectively. This observation can be rationalized in terms of radiative and radiationless recombination of trapped carriers. At low temperatures, both processes occur exclusively via a tunneling mechanism.

A noteworthy feature of the luminescence of CdS and other II–VI or III–V semiconductors is that it is extremely sensitive to the presence of electron acceptors such as MV^{2+} or benzoquinone. In water, a concentration of 10^{-8} M of MV^{2+} suffices to quench 50% of the red emission of CdS.[57] A quantitative analysis of the results, using Poisson statistics to describe the quencher distribution over the particles, showed that only one MV^{2+} molecule per aggregate is required to quench the emission.[57] The role of the MV^{2+} is to scavenge conduction band electrons, intercepting, in this way, their radiative and nonradiative recombination with holes. Recent laser photolysis experiments with picosecond time resolution have shown that this reaction is very fast requiring less than a nanosecond.[76–78]

2.3. Electronic Properties

2.3.1. Band Edge Positions

In Figure 3 are given band gaps and band edge positions for a number of ionic and covalent materials in the bulk state. The data refer to conditions where the semiconductor is in contact with aqueous redox electrolytes of pH 1. Knowledge of the band positions or flat band potentials is useful in as much as they indicate the thermodynamic limitations for the photoreactions that can be carried out with the charge carriers. For example, if a reduction of the species in the electrolyte is to be performed, the conduction band position of the semiconductor has to be positioned above the relevant redox level. It should be noted, however, that the ordinate in Figure 3 presents internal energy and not free energy. The free energy of an electron–hole pair is smaller than the energy of the band gap. The reason for this behavior is that the electron–hole pairs have a significant configurational entropy arising from the large number of translational states accessible to the mobile carriers in the conduction and valence band.

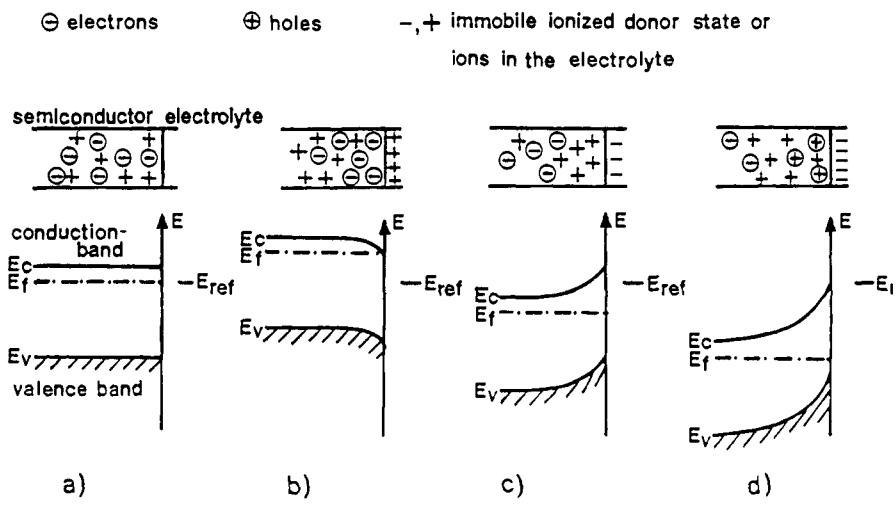

Figure 4. Space charge layer formation at the n-type semiconductor–solution interface: (a) flat band situation, (b) accumulation layer, (c) depletion layer, and (d) inversion layer.

2.3.2. Space Charge Layers and Band Bending

The generation of a space charge layer requires the transfer of mobile charge carriers between the semiconductor and the electrolyte. For bulk semiconductors in contact with a liquid medium, the charge transfer can only take place in the presence of an electroactive species acting as electron donor or acceptor. Thus, an interfacial redox reaction is required to produce the electric field within the semiconductor. Within the space charge layer the valence and conduction bands are bent. Here, four different situations may be envisaged. These are illustrated in Figure 4 for an n-type semiconductor in contact with an electrolyte. If there is no space charge layer, the electrode is at the flat band potential. If charges are accumulated at the semiconductor side which have the same sign as the majority charge carriers, one obtains an accumulation layer. If, on the other hand, majority charge carriers deplete into the solution, a depletion layer is formed. The excess space charge within this layer is given by immobile ionized donor states. The depletion of majority carriers can go so far that their concentration at the surface decreases below the intrinsic level. If the electronic equilibrium is maintained the concentration of holes in this region of the space charge layer exceeds that of electrons. As a consequence, the Fermi level is closer to the valence than the conduction band and the semiconductor is p-type at the surface and n-type in the bulk. This is called an inversion layer.

The situation is different in a colloidal semiconductor or in a nanocrystalline network. The potential distribution in a spherical semiconductor particle has been derived by Albery and Bartlett[79] using a linearized Poisson–Boltzmann equation. They obtain for the difference in the potential at the center ($r = 0$) and at a distance r the relation:

$$\Delta\phi_{sc} = \frac{kT}{6e}\left(\frac{r - (r_0 - W)}{L_D}\right)^2\left(1 + \frac{2(r_0 - W)}{r}\right) \quad (10)$$

where $L_D = (\epsilon_0\epsilon kT/2e^2N_D)^{0.5}$ is the Debye length which depends on the number of ionized dopant molecules per cubic centimeter, N_D, $\Delta\phi_{sc}$ is the potential drop

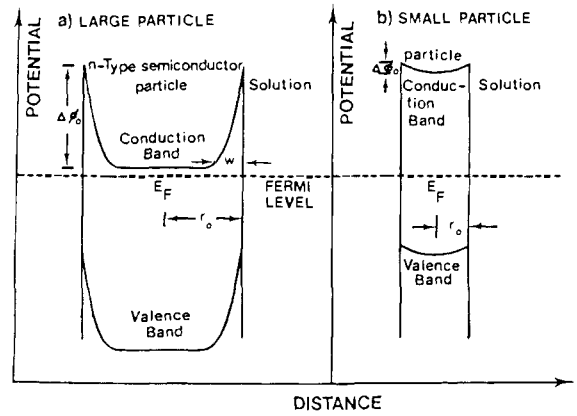

Figure 5. Space charge layer formation in a large and small semiconductor particle in equilibrium with a solution redox system for which the Fermi level is E_F. The small particle depletes almost completely of charge carriers. Hence, its Fermi potential is located approximately in the middle of the band gap and band bending is negligibly small.

within the layer, and W is the width of the space charge layer. A graphic illustration of the potential distribution for an n-type semiconductor particle, which is in equilibrium with a solution containing a redox system for which the Nernst potential is E_f, is shown in Figure 5. Two limiting cases of eq 10 are particularly important for light-induced electron transfer in semiconductor dispersions. For large particles, the total potential drop within the semiconductor is

$$\Delta\phi_0 = \frac{kT}{2e}\left(\frac{W}{L_D}\right)^2 \quad (11)$$

which is the same as for planar electrodes. For very small (colloidal) semiconductor particles, the total potential drop within the semiconductor becomes

$$\Delta\phi_0 = \frac{kT}{6e}\left(\frac{r_0}{L_D}\right)^2 \quad (12)$$

From this equation and Figure 5 it is apparent that the electrical field in colloidal semiconductors is usually small and that high dopant levels are re-

quired to produce a significant potential difference between the surface and the center of the particle. For example, in order to obtain a 50 mV potential drop in a colloidal TiO_2 particle with $r_o = 6$ nm, a concentration of 5×10^{19} cm^{-3} of ionized donor impurities is necessary. Undoped TiO_2 colloids have a much smaller carrier concentration and the band bending within the particles is therefore negligibly small. If majority carriers deplete from a colloidal semiconductor in solution and the particles are too small to develop a space charge layer the electrical potential difference resulting from the transfer of charge from the semiconductor to the solution has to drop within the Helmholtz layer, neglecting diffuse layer contributions. As a consequence, the position of the band edges of the semiconductor particles will shift. The same considerations hold for the transfer of minority carriers formed by photoexcitation of the semiconductor particles. For example if after photoexcitation of a colloidal n-type, particle holes are transferred rapidly to an acceptor in solution while electrons remain in the particle a negative shift in the conduction band edge at the surface will take place.

2.3.3. Light-Induced Charge Separation

The depletion layer at the interface between a bulk semiconductor and a liquid medium, plays an important role in light-induced charge separation. The local electrostatic field present in the space charge layer serves to separate the electron–hole pairs generated by illumination of the semiconductor. For n-type materials, the direction of the field is such that holes migrate to the surface where they undergo a chemical reaction, while the electrons drift through the bulk to the back contact of the semiconductor and subsequently through the external circuit to the counter electrodes. Charge carriers which are photogenerated in the field-free space of the semiconductor can also contribute to the photocurrent. In solids with low defect concentration the lifetime of the electron–hole pairs is long enough to allow for some of the minority carriers to diffuse to the depletion layer before they undergo recombination.

In the case of colloidal semiconductors, the band bending is small and charge separation occurs via diffusion. The absorption of light leads to the generation of electron–hole pairs in the particle which are oriented in a spatially random fashion along the optical path. These charge carriers subsequently recombine or diffuse to the surface where they undergo chemical reactions with suitable solutes or catalysts deposited on the surface of the particles. Applying a random walk model in order to describe the motion of the charge carriers one obtains for the average transit time from the interior of the particle to the surface the expression:

$$\tau_d = \frac{r_0^2}{\pi^2 D} \tag{13}$$

For colloidal semiconductors τ_d is at most a few picoseconds. Thus for colloidal TiO_2 ($D_{e^-} = 2 \times 10^{-2}$ cm^2/s) with a radius of 6 nm the average transit time of the electron is 3 ps.

In the presence of a depletion layer, the transit time of the minority carriers is further reduced since, in this case, the Debye length has to be used in eq 13 instead of the particle radius.[80] However, the potential difference between particle surface and interior has to be at least 50 mV in order for migration to dominate over diffusion.

It should be noted that the random walk model breaks down for particles exhibiting quantum size effects. Here, the wave function of the charge carrier spreads over the whole semiconductor cluster and they do not have to undergo diffusional displacement to accomplish reactions with species present at the surface.

Since in colloidal semiconductors the diffusion of charge carriers from the interior to the particle surface can occur more rapidly than their recombination, it is feasible to obtain quantum yields for photoredox processes approaching unity. Whether such high efficiencies can really be achieved, depends on the rapid removal of at least one type of charge carrier, i.e. either electrons or holes, upon their arrival at the interface. This underlines the important role played by the interfacial charge transfer kinetics which we shall treat in further detail below.

2.4 Charge Carrier Reactions in Colloidal Semiconductor Solutions

2.4.1 Dynamics of Interfacial Charge Transfer Processes

Consider the reaction of conduction band electrons or valence band holes produced by excitation of a colloidal semiconductor particle with an appropriate acceptor molecule in solution. In the latter case, the overall reaction is composed of two steps (Figure 6):

(i) Encounter complex formation of the electron (or hole) acceptor with these semiconductor particle. The rate of this process is diffusion-limited and hence determined by the viscosity of the medium and the radius of the particle.

(ii) Interfacial electron transfer. This electrochemical step involves a Faradaic current across the semiconductor/solution interface and is characterized by the rate parameter k_{ct} (units cm/s). Neglecting surface charge effects on the approach of the reactants, the latter is related to the observed bimolecular rate constant via[55]

$$\frac{1}{k_{obs}} = \frac{1}{4\pi R^2}\left(\frac{1}{k_{ct}} + \frac{R}{D}\right) \tag{14}$$

where R is the sum of the radii of the semiconductor particle and electron (or hole) acceptor and D is the sum of their respective diffusion coefficient. The structure of this equation suggests two limiting cases:

Heterogeneous charge transfer is rate determining and much slower than diffusion ($k_{ct} \ll D/R$). In this case eq 14 reduces to

$$k_{obs} = 4\pi R^2 k_{ct} \tag{15}$$

(ii) Heterogeneous charge transfer is faster than diffusion, which controls the overall reaction rate ($k_{et} \ll D/R$). In this case we obtain from eq 14 the well-

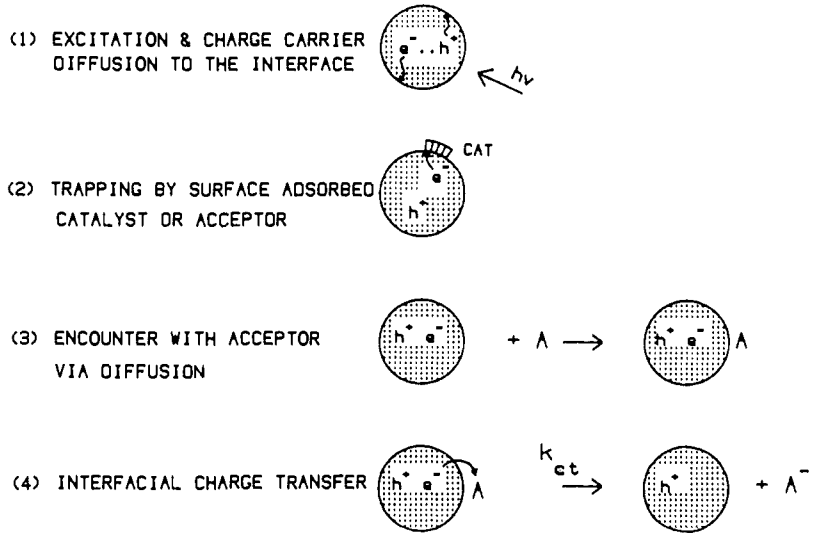

Figure 6. Elementary steps in the heterogeneous electron transfer induced by light from a semiconductor particle to an acceptor or a catalyst.

known Smoluchowski expression:

$$k_{obs} = 4\pi DR \tag{16}$$

Note, finally, that the diffusion effects can be eliminated by adsorption or chemical fixation of the acceptor at the semiconductor particle surface. Here the simple reaction:

$$k_{ct} = \delta/\tau_{ct} \tag{17}$$

holds where τ_{ct} is the average time required for the charge carrier to tunnel across the interface and δ is the reaction layer thickness.

In the following we illustrate how heterogeneous rate constants for electron transfer from colloidal semiconductors to acceptors in solution can be determined experimentally. Methyl viologen (MV^{2+}, E° = −0.44 V vs NHE) has been widely used as electron acceptor in these studies. The free energy of the charge transfer reaction

$$e_{cb}^{-}(TiO_2) + MV^{2+} \rightarrow MV^{+} \tag{18}$$

is pH dependent since the flat band potential of TiO_2 changes with pH. Thus, the heterogeneous rate constant k_{ct} also depends on the solution pH. Expressing k_{ct} with a Tafel relation one obtains for the observed rate constant:[81]

$$\frac{1}{k_{obs}} = \frac{1}{4\pi R^2}\left(\frac{1}{k_{ct}^{0}\, 10^{(\alpha[0.11+0.059\times pH+E^{0}(A/A^{-})]F/RT)}} + \frac{r}{D}\right) \tag{19}$$

The kinetic treatment of interfacial electron transfer reactions presented so far neglects Coulombic effects in the diffusional approach of semiconductor particle and acceptor. Therefore eq 19 is only valid when electrostatic work terms are negligible, i.e. the acceptor and/or particle is unchanged or the ionic strength is high. In general, eq 19 must be corrected[85,86] to allow for variation in electrostatic attraction as the pH changes. For example, in the case of the reduction of MV^{2+} by conduction band electrons of colloidal TiO_2, Brown and Darwent found empirically:[85]

$$\log k_{ct} = \log k_0 + \left(\alpha + \frac{\gamma}{\sqrt{I}}\right) pH + \frac{\gamma}{\sqrt{I}} PZZP \tag{20}$$

where $\gamma \cong 0.04$ is a constant, I is the ionic strength, and PZZP the point of zero ζ potential of the particle. Equation 20 shows that for low ionic strength the slope of the d log k_{ct}/dpH plot is increased and does not correspond straightforwardly to the transfer coefficient α.

The reciprocal average time for interfacial electron transfer may be expressed in terms of the Marcus relation for nonadiabatic electron transfer:

$$\frac{1}{\tau_{ct}} = \nu_0 \exp[-\beta(d-d_o)] \exp\left(\frac{(\Delta G^{*}+\lambda)^2}{4\lambda kT}\right) \tag{21}$$

The parameter ν_0 is the frequency factor reflecting the rate constant of electron transfer for optimal exothermicity when the species are in contact ($d-d_o$). Assuming that at room temperature n_o has a value of ca. $10^{13.3}$ s^{-1} and that interfacial charge transfer occurs over a distance of $d-d_o$ = 4 Å, one obtains from eq 21 $k_1 = 5 \times 10^{10}$ s^{-1} when $\beta = 1.2$ $Å^{-1}$ and the driving force is optimal ($-\Delta G^{*} = \lambda$). If $\Delta G^{*} = 0$ and the reorganization energy $\lambda = 0.5$ eV, k_1 equals 3.4×10^9 s^{-1}. Since the reaction layer has a thickness of about $1/\beta \simeq 0.8$ Å, the heterogeneous rate constant at zero driving force $k_{ct}^{\circ} = 2.7$ cm/s is obtained.

The k_{ct}° values reported in the literature so far are smaller than this limit indicating $\lambda > 0.5$ eV and/or $d > 5$ Å for the acceptors investigated. It should be noted that very high electron transfer rates ($k_1 > 10^8$ s^{-1}) were obtained in cases where the acceptor adheres strongly to the surface of the semiconductor. Examples are the one-electron reduction of dimeric viologens adsorbed onto colloidal TiO_2 which is completed within 50 ps after laser excitation of the particles and the reduction of MV^{2+} by conduction band electrons of CdS.[67,76,82-84] A detailed analysis

of the kinetics of charge transfer reactions at the semiconductor–solution interface has recently appeared.[87]

According to eq 14 the rate constant for charge transfer between a semiconductor particle and a species in solution is size dependent. Frequently, in a colloidal dispersion there is a distribution of particle sizes. Semiconductor particles having a different radius should react with different rate constants. The larger particles should react at a faster rate than the smaller ones. Such effects have indeed been observed.[88] Under pseudo-first-order conditions, where an exponential rate law is expected, polydispersity of the colloidal manifests itself by nonlinearity of the semilogarithmic plots, positive deviations occurring at longer times. A good curve fitting was obtained by assuming a Gaussian distribution of particle size.

2.4.2 Effect of Surface Chelation on the Rate of Interfacial Electron Transfer Reactions

Surface complexation of colloidal titanium dioxide by monodentate and bidentate benzene derivatives, i.e. benzoic acid, *o*-, *m*-, and *p*-phthalic acid, salicylate, and catechol, was investigated and was found to obey the Langmuir isotherm.[3] The adsorption constants in aqueous/methanol mixtures (90/10, v/v) at pH 3.6 decrease from 2×10^5 for *p*-phthalate to 2×10^3 for benzoate. Electrophoretic measurements show the adsorption to be accompanied by a decrease of the point of zero ζ potential (PZZP), the shift observed for salicylate being 0.5 units. At pH 3.6, the influence of the adsorbate on the ζ potential of the TiO_2 particles is relatively small. The largest effect is observed with *m*-phthalate which decreases *z* from 78 to 51 mV. Laser photolysis experiments indicate that surface complexation of TiO_2 by these benzene derivatives drastically accelerates the electron transfer from the conduction band of the colloidal oxide to acceptors in solution, i.e. methylviologen (MV^{2+}) and oxygen. The rate enhancement depends greatly on the structure and chemical nature of the adsorbate. At monolayer coverage, *m*-phthalate enhances the rate of interfacial electron transfer to MV^{2+} 1700 times while *p*-phthalate gives a 133-fold rate increase. Monodentate benzoate accelerates the interfacial electron transfer only by a factor of 3. Similar effects were observed for oxygen as electron acceptor. Trapping of electrons by Ti(IV) surface states and the removal of such traps by complexation with the benzene derivatives is evoked to rationalize these observations.

2.4.3 Photosensitized Electron Injection in Colloidal Semiconductors

The photosensitization of electron transfer across the semiconductor solution interface plays a vital role in silver halide photography[89] and electroreprography.[90] Recently, it has also gained interest with regard to information storage and light energy conversion in photoelectrochemical cells.[91] In these systems, the phenomenon of photosensitized electron injection is used to effect charge separation with light of less than band gap energy. Of particular importance for the development of artificial photosynthetic devices is the sensitization of semiconducting oxides such as TiO_2,[92] SnO_2,[93] and ZnO.[94]

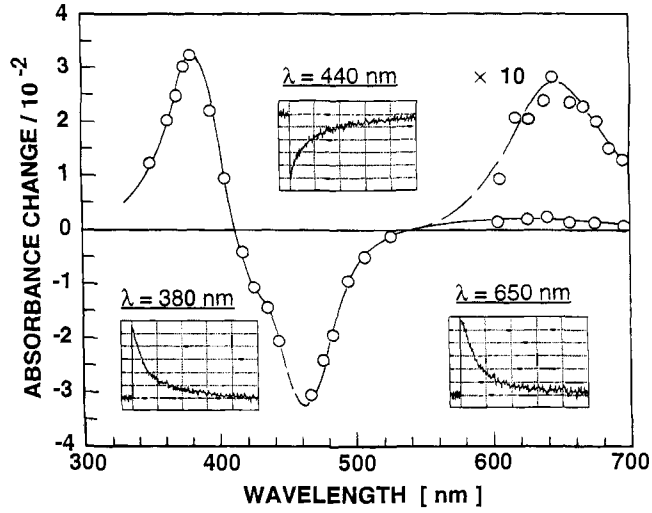

Figure 7. Laser photolysis of coumarin 343 loaded TiO_2 colloids; transient absorption spectrum obtained immediately after pulsed 450 nm laser excitation of the adsorbed coumarin. The insets show the temporal behavior of the absorption at three different wavelengths to illustrate the time course of the back-electron transfer from the conduction band of the colloidal particle to the coumarin cation radical.

While much pertinent information has been gathered over the years on the overall performance of dye-sensitized semiconductor systems, more precise data about the details of the electron injection and recapture process are urgently required. The rapid nature of these reactions requires application of fast kinetic techniques which, in the case of solid semiconductor electrodes or powders, is very difficult. On the other hand, the dynamics of electron injection can readily be investigated with colloidal semiconductors by application of flash photolysis. In the following, we discuss the salient kinetic features of interfacial electron transfer processes associated with sensitization. A system that has recently been investigated consists of colloidal TiO_2 as a semiconductor and coumarin 343 as a sensitizer.[95,96] This is used as an example to illustrate the dynamics of the sensitization process. Figure 7 shows time-resolved laser studies with an ethanolic solution of colloidal TiO_2 onto which the coumarin has been adsorbed. The dye is excited with 450 nm output of a pulsed dye laser and the absorbance change observed immediately after the laser excitation is plotted as a function of detection wavelength. There are three features in the transient absorption spectrum: a bleaching signal at 460 nm and absorption peaks at 380 and 650 nm which are attributed to the coumarin ground state the coumarin radical cation and the conduction band electrons, respectively. This indicates that the electron injection from the coumarin into the conduction band occurs during and within the laser pulse.

$$\text{coumarin} + h\nu \rightarrow \text{coumarin}^{+} + e^{-}_{cb} \quad (22)$$

Recent femtosecond studies showed the injection time to be around 160 fs. The cation radical is formed with a yield of practically 100%.[96] The subsequent recombination occurs over a much longer time scale, i.e. several microseconds as shown by the insets of Figure 6. Because electron injection occurs on the picosec-

ond time scale it is several thousand times faster than charge recombination. Thus light-induced charge separation is very efficient for this system and is sustained on the colloidal TiO_2 particle for several microseconds.

Similar effects have been observed very recently with a number of different sensitizers such as porphyrins[97] and $Ru(bipy)_3^{2+}$ derivatives[98] or $Fe(CN)_6^{4-}$ surface derivatized TiO_2 particles.[99] In all these cases the back-electron transfer from the semiconductor particle to the oxidized sensitizer occurred with a rate that was several orders of magnitude slower than the forward injection. Thus, the combination of a sensitizer with a colloidal semiconductor particle affords a molecular device for light-induced charge separation. The question should be addressed why in this system the rate of the back-reaction is so much smaller than that of the forward electron transfer. One might evoke the fact that recapture of the conduction band electron has a large driving force placing this reaction in the inverted region where the rate drops with increasing exothermicity. In addition, entropic factors should be considered. In a 120 Å sized TiO_2 particle, the electron is delocalized over 3600 conduction band states. If there is only one sensitizer cation available at the surface, the back-reaction is associated with a significant entropy decrease which amounts to ca. 16 cal/(K mol). This favorable charge separation in the sensitization of oxide semiconductors has recently found an application in the conversion of light to electricity by regenerative photoelectrochemical cells.[98,100,101]

On the basis of these findings a new molecular photovoltaic system for solar light harvesting and conversion to electricity has been developed. This system will be described in the next section.

3. Nanocrystalline Semiconductor Electrodes

To take advantage of the properties of nanometer-sized semiconductor particles for light-to-electrical energy conversion, a pathway for electrical conduction between the particles must be provided. Two processing routes have been reported in the literature. In the first approach, particles are applied to a conducting substrate from a suspension and then sintered to form electrical contact between the particles and to allow for charge transport to the substrate.[54] In the second approach, nanocrystalline particles are formed directly onto the substrate by an electrochemical or chemical deposition process.[102] The nanocrystalline semiconductor electrodes distinguish themselves by their porosity and high surface-to-volume ratio. A scanning electron micrograph illustrating the mesoporous morphology of such a nanocrystalline semiconductor oxide film is shown in Figure 8. Today, the most promising device for solar light-to-electrical conversion is a photosensitized titanium dioxide nanocrystalline electrode with Ru–bipyridyl complexes.[100,101,103–106] For example, bis(bipyridyl)Ru^{II} complexes having the general formula *cis*-X_2bis(2,2′-bipyridyl-4,4′-dicarboxylato)ruthenium(II), where X = Cl^-, Br^-, I^-, CN^-, and SCN^- have been developed. A systematic study of their luminescence, visible light absorption, electrochemical, and photoredox behavior was performed[101] and among

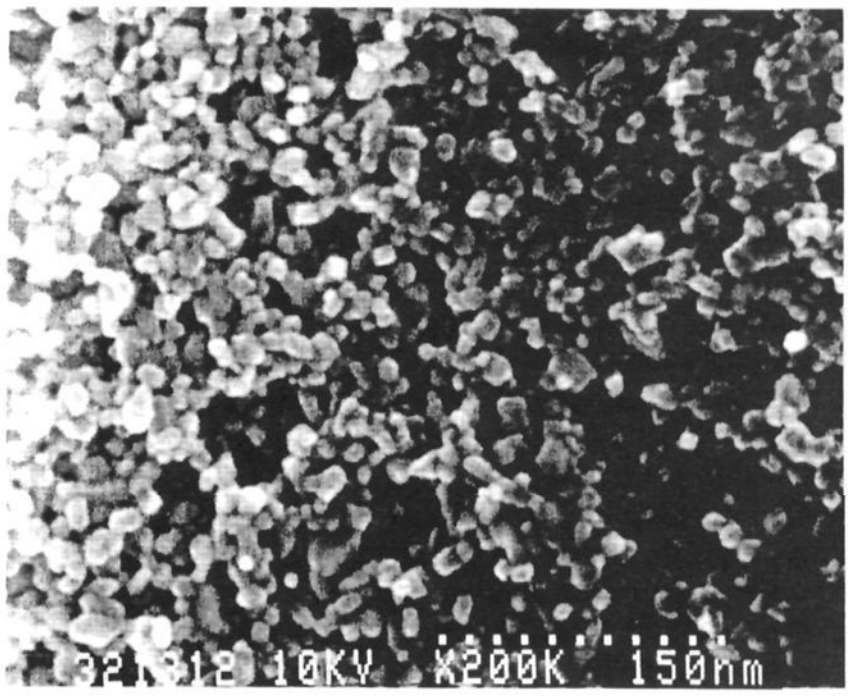

Figure 8. Scanning electron micrograph showing the nanocrystalline TiO_2 films deposited on conducting glass. Scales indicated on the photograph. See text and refs 100 and 101 for further details.

these compounds, *cis*-bis(thiocyanato)bis(2,2′-bipyridyl-4,4′-dicarboxylato)ruthenium(II), $RuL_2(SCN)_2$, performs as an outstanding solar light absorber and charge-transfer sensitizer, unmatched by any other dyestuff known so far. The photosensitization of wide band gap semiconductors such as TiO_2 by adsorbed dyes has been studied since the late 1960s. In fact dye sensitization of semiconductors can be traced back to the early days of photography. For an historical overview of photosensitization of semiconductors see ref 4. The earlier photoelectrochemical studies focused on flat electrodes, but these systems were facing an intrinsic problem. Only the first monolayer of adsorbed dye results in efficient electron injection into the semiconductor, but the light-harvesting efficiency of a single dye monolayer is very small. In a porous film consisting of nanometer-sized TiO_2 particles, the effective surface area can be enhanced 1000-fold, thus making light absorption efficient even with only a dye monolayer on each particle. Nature, in fact, uses a similar means of absorption enhancement by stacking the chlorophyll-containing thylakoid membranes of the chloroplast to form the grana structures. (There are actually several interesting analogies between the natural photosynthesis and the dye-sensitized nanocrystalline semiconductor electrode, which we will point out throughout the text.) An intriguing feature in the nanocrystalline TiO_2 films is that the charge transport of the photoinjected electrons passing through all the particles and grain boundaries is highly efficient, the quantum yields being practically unity.[101,107] In recent years, therefore, considerable interest has been shown in developing thin semiconductor films from colloidal suspensions for photovoltaic devices (cf. ref 108). But other possible applications such as electrochromic effects,[109–112] photoconductors,[113–115] and light-activated catalysts[116,117] have been explored. There have also been several efforts to employ nanocrystalline semiconductor films for the photocatalytic degradation of organic contaminants. Some of these works can be found in refs 116,118–123.

An alternative approach to dye adsorption for photosensitization of wide band gap semiconductors is to deposit a thin layer of narrow band gap semiconductor materials. Quantum-sized particles have been deposited onto nanoporous semiconductor films and those modified layers have been used as light-converting electrodes. For example, CdS,[124,125] CdSe,[126,127] PbS,[125] and FeS_2[128] have been deposited on nanocrystalline TiO_2 films. In an extensive study by Vogel et al.[125] it was shown that the relative positions of the energetic levels at the interface between the quantum-size particles and the oxide substrate can be optimized for an efficient charge separation by utilizing the size quantization effect and by varying the materials of the particles and the substrate. The text will focus on the TiO_2 and the dye-sensitized TiO_2 nanocrystalline electrode, since these systems up to now have been the most studied, but other materials to prepare nanoporous electrodes have also been investigated: ZnO,[125,129-131] CdSe,[102] CdS,[102,132] WO_3,[109] Fe_2O_3,[133] SnO_2,[125,134] Nb_2O_5,[125] and Ta_2O_5.[125] It will be show that a conventional way of treating photoelectrochemical systems, e.g. in terms of Schottky junctions, the charge carriers being separated in the semiconductor space charge layer, etc., is not applicable to nanocrystalline semiconductor junctions. It is perhaps better to discuss the nanoporous films in colloidal concept, i.e. the charge separation being mainly controlled by kinetics at the semiconductor/electrolyte interface (SEI), etc. Interestingly it has been found that nanocrystalline films with particle sizes commensurate or smaller than their Bohr radius exhibit quantum size properties.[102,109,130,132] This means that there is a potential barrier between the particles[130] and that the particles constituting the film can, in some respect, be regarded as individual entities. The finding that many of these systems show very high quantum yields is than even more remarkable. Trying to understand these features from a fundamental point of view is the task of this section. Common characteristics in the operations of nanocrystalline TiO_2 electrodes are the filling of trap states and that the charge separation process is mainly governed by the kinetics at the SEI. On the basis of these findings the success in using dye-sensitized colloidal TiO_2 films as solar cells can be explained and improvements and possibilities of the photovoltaic cell will be addressed.

3.1. Some Basic Properties and Preparation Procedures of Nanocrystalline TiO_2 Films

The preparation of nanoporous TiO_2 films have been described in detail.[100,101] The electrodes are prepared by spreading a paste of nanosized colloidal TiO_2 particles on a conducting glass support (TCO contact). Sintering at 350–450 °C produces electronic contact not only between the particles and the support but also between practically all the particles constituting the film. Thus a sponge-like structure is obtained and the colloidal TiO_2 film is porous (typically a porosity of 50% is achieved) from the outer layers to the TCO contact. The pores between the colloidal particles are interconnected and can be filled with an electrolyte, i.e. the SEI is accessible throughout the whole colloidal membrane. A roughness factor, defined as the ratio between the real and projected surface of these films, of about 1000 has been estimated for a 10 μm thick TiO_2 film. It should be pointed out that the porosity of the film can vary with the sintering temperature dependent on the material. For example ZnO nanocrystalline films can be made with a high porosity at sintering temperatures of about 200 °C, whereas a more compact film is obtained after sintering at 400 °C.[135] Care should therefore be taken in interpreting colloidal semiconductor films with respect to their porosity. In this context we would also like to mention that the optical properties of the nanophase TiO_2 films can be drastically changed due to the autoclaving step in the preparation procedure (cf. ref 101) with implements for different devices. The purpose of the autoclaving step is to increase the particle size and hence better diffusion properties in the electrolyte. Autoclaving the colloidal solution at 200 °C yields a transparent nanocrystalline TiO_2 (100% anatase) film with a relatively uniform particle size distribution of 15 nm. Increasing the autoclaving temperature to 250 °C gives a film showing a high degree of light scattering. In this white film aggregates of small particles and usually some larger particles (>100 nm) are found and there is some content of rutile. To produce film thicknesses above 5 μm and for better ion diffusion in the electrolyte it is, according to our experience, an advantage if aggregates and/or larger particles are included in the colloidal paste. Therefore, the photovoltaic cell is usually based on a 240–250 °C autoclaved colloidal solution with a film thickness of 10 μm, whereas the electrochromic electrode in refs 111 and 112 is made from a solution autoclaved at 200 °C giving a transparent 3–4 μm thick film.

3.2. Energetics and Operations of the Nanoporous Solar Cell

A schematic drawing of the energy levels of a dye-sensitized nanocrystalline TiO_2 film in contact with an electrolyte is shown in Figure 9. The desired pathway for a photoexcited electron in a photovoltaic cell is also indicated. As an example we have used the $RuL_2(SCN)_2$ dye adsorbed on TiO_2 with a I^-/I_3^- containing electrolyte (cf. ref 101). Dye-sensitized cells differ from the conventional semiconductor devices in that they separate the function of light absorption from charge carrier transport. The role of the ruthenium complex is the same as that of chlorophyll in the green leaf: it must absorb the incident sunlight and exploit the light energy to induce a vectorial electron transfer reaction. Very promising results have so far been obtained with Ru complexes where at least one of the ligands was 4,4′-dicarboxy-2,2′-bipyridyl. The carboxylates serve to attach the Ru complex to the surface of the oxide and to establish good electronic coupling between the π^* orbital of the electronically excited complex and the 3d wave function manifold of the TiO_2 film. The substitution of the bipyridyl with the carboxylate groups also lowers the energy of the π^* orbital of the ligand. Since the electronic transition in the dye is of metal to ligand charge transfer (MLCT) character the excitation energy is channeled into the right ligand, i.e. the one from which electron injection into the conduction band takes place.

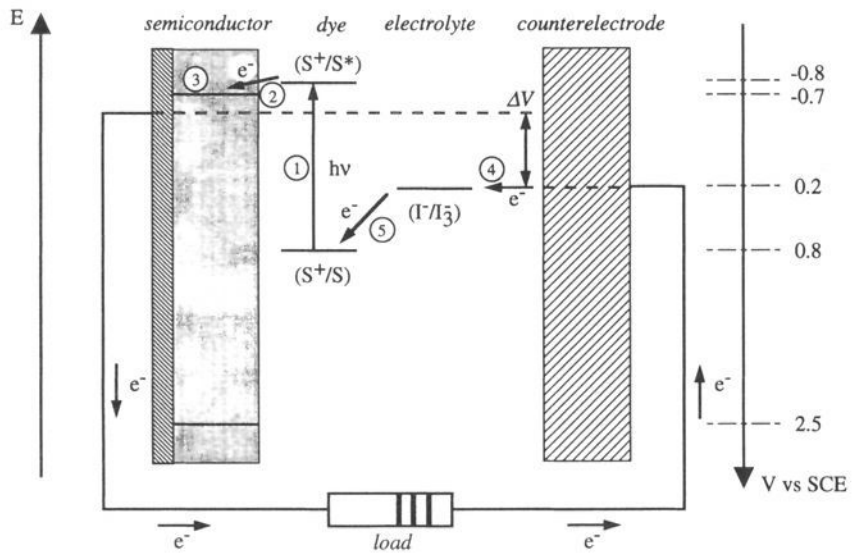

Figure 9. Schematic representation of the principle of the dye-sensitized photovoltaic cell to indicate the electron energy level in the different phases. Also indicated on the potential axis are the values of the different electronic levels for the photovoltaic cell developed in ref 101. This system consists of the $RuL_2(SCN)_2$ dye adsorbed on TiO_2 and the I^-/I_3^- redox couple in the electrolyte (see text for further details). The value of the redox potential (0.2 V vs SCE) is the formal potential in the solution whereas the value of the oxidation potential of the dye is the standard potential. The absorption threshold for the $RuL_2(SCN)_2$ dye adsorbed on TiO_2 is about 800 nm corresponding to a potential of 1.6 V (neglecting the entropy contribution), which added to the oxidation potential of the dye gives a reduction potential of −0.8 V vs SCE. From the potential of the conduction band edge, V_{cb}, and the band gap energy of 3.2 eV of TiO_2 (anatase) the potential of the valence band edge is obtained. The cell voltage observed under illumination corresponds to the difference, ΔV, between the quasi-Fermi level of TiO_2 and the electrochemical potential of the electrolyte. S stands for sensitizer; S*, electronically excited sensitizer; S^+, oxidized sensitizer.

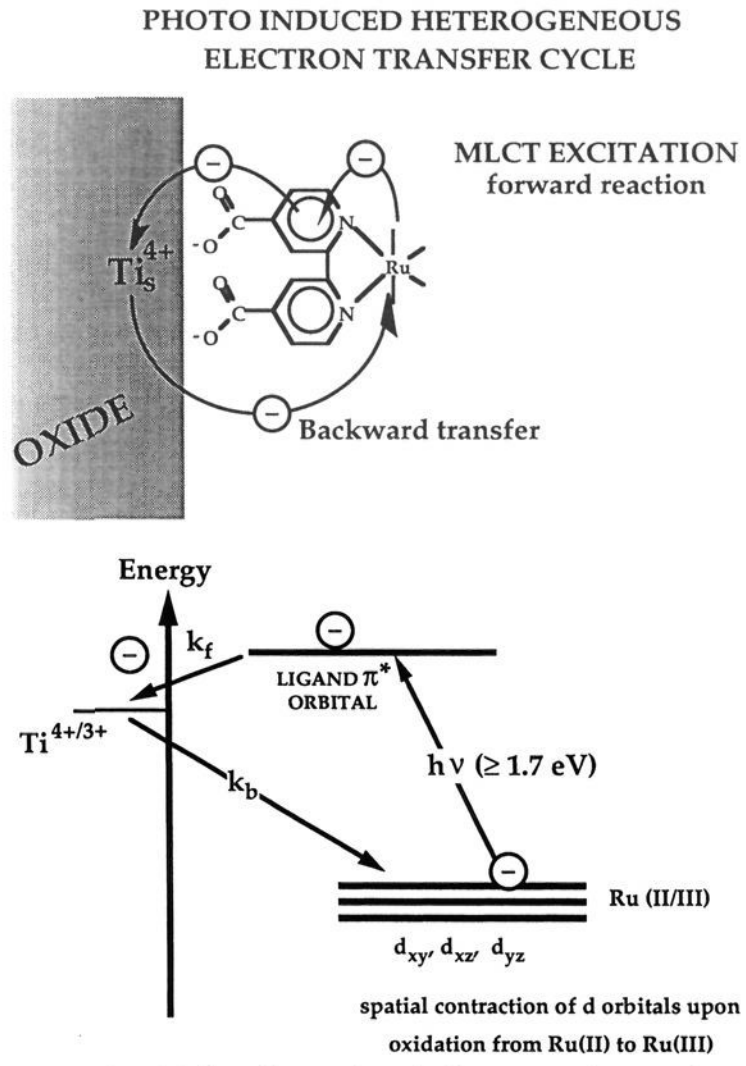

Figure 10. Molecular orbital diagram for ruthenium complexes anchored to the TiO_2 surface by a carboxylated bipyridyl ligand. The visible light absorption of these types of complexes is a metal-to-ligand charge transfer (MLCT) transition. The carboxylate groups are directly coordinated to the surface titanium ions producing intimate electronic contact between the senitizer and the semiconductor.

In place of the biological lipid membrane in the green leaf a TiO_2 film is employed. Apart from acting as a support for the sensitizer, it also functions as electron acceptor and electronic conductor. The electrons injected by the sensitizer into the TiO_2 conduction band travel across the nanocrystalline film to the conducting glass support serving as current collector, see Figure 9. The driving force necessary for the rapid vectorial charge diplacement is small. It corresponds to about 0.1 eV required to drive the electron injection process. To complete the circuit, the dye must be regenerated by electron transfer from a redox species in solution which is then reduced at the counter electrode. We note that this cell is not a minority carrier device since the photogenerated hole remains localized on the oxidized dye molecule. In conventional p−n junctions a long minority carrier diffusion length is essential, thus pure and well-ordered semiconductor materials are required. In the dye-sensitized nanocrystalline cell recombination can occur only at the interface, where the injected electrons can recombine with oxidized dye molecules or with oxidized species in the electrolyte. For the characterization of the recombination rate, an important kinetic parameter is the rate constant k_b, see Figure 10. It is of great interest to develop sensitizer systems for which the value of the electron injection, k_{inj}, is high and that of k_b low. Fortunately, for the transition metal complexes we use, the ratio of injection over recapture rate k_{inj}/k_b is greater than 10^3. In some cases it even exceeds one million. The reason for this behavior has been discussed in section 2.4.3. What can be added here is that the molecular orbitals involved in the back-reaction overlap less favorably with the wave function of the conduction band electron than those involved in the forward process. For example, for $RuL_2(SCN)_2$ bound to the nanocrystalline oxide film, the injecting orbital is the π^* wave function of the carboxylated bipyridyl ligand. The carboxylate groups interact directly with the surface Ti(IV) ions resulting in good electronic coupling of the π^* wave function with the 3d orbital manifold of the conduction band of the TiO_2. As a result, the electron injection from the excited sensitizer into the semicondcutor membrane is an extremely rapid process occurring in less than a picosecond, see Figure 10. By contrast, the back-reaction of the electrons with the oxidized ruthenium complex involves a d orbital localized on the ruthenium metal whose electronic overlap with the TiO_2 conduction band is small. The spatial contraction of the wave function upon oxidation of the Ru(II) to the Ru(III) state further reduces this electronic coupling. This, together with the fact that the driving force for the back-electron transfer is large enough to place it in the inverted Marcus domain explains the relatively slow backward electron transfer which, typically, is in the microsecond time domain. Thus, in analogy to natural photosynthesis, light-induced charge separation is achieved on kinetic grounds, the forward electron transfer being orders of magnitude faster than the back reaction. As a consequence, the presence of a local

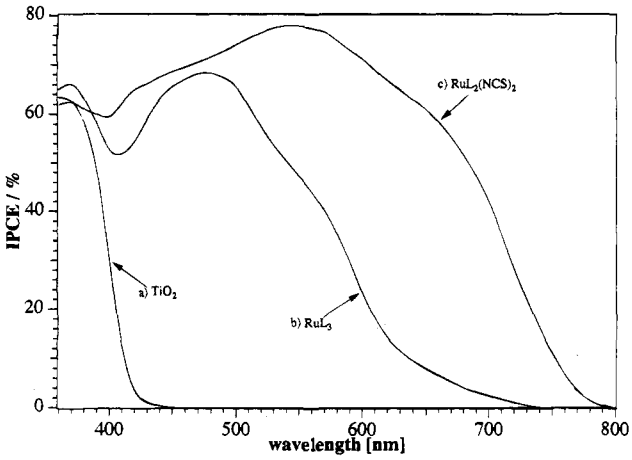

Figure 11. Photocurrent action spectrum obtainded with two different ruthenium-based sensitizers attached to the nanocrystalline TiO_2 film. The blank spectrum obtained with the bare TiO_2 surface is shown for comparison. The incident photon-to-current conversion efficiency is plotted as a function of excitation wavelength. The IPCE values are not corrected for the loss of light intensity due to absorption and reflection by the conducting glass support. The size of the working electrode was ca 0.5 cm^2. The counter electrode was a conducting glass electrode covered with a transparent film of Pt. The cell was operated in the short-circuit mode.

electrostatic field is not required to achieve good efficiencies for the process.

The incident monochromatic photon-to-current conversion efficiency (IPCE) is defined as the number of electrons generated by light in the external circuit divided by the number of incident photons. A graph which presents the monochromatic current output as a function of the wavelength of the incident light is called the "photocurrent action spectrum". Figure 11 shows such action spectra for two ruthenium complexes, illustrating the very high efficiency of current generation, exceeding 75% obtained with these complexes. When corrected for the inevitable reflection and absorption losses in the conducting glass serving to support the nanocrystalline film, yields of practically 100% are obtained. Historically, RuL_3 (L = 2,2'-bipyridyl-4,4'-dicarboxylate) was the first efficient and stable charge transfer sensitizer to be used in conjunction with high surface area TiO_2 films.[98] In a long-term experiment carrier out during 1988 it sustained 9 months of intense illumination without loss of performance. However, the visible light absorption of this sensitizer is insufficient for solar light conversion. The most successful charge transfer sensitizer investigated so far is without any doubt $RuL_2(SCN)_2$. It accomplishes close to quantitative photon to electron conversion over the whole visible range.[101] Even at 700 nm current generation is still 40−50% efficient.

The photovoltage of the nanocrystalline solar cell cell represents the difference between the Fermi level of titanium dioxide under illumination and the redox potential of the electrolyte (Figure 9). Using the triiodide/iodide redox couple, in e.g. *N*-methyloxazolidinone solution, under full sunlight an open-circuit cell voltage of 0.7−0.9 V can be measured. Under a 1000-fold lower intensity the cell voltage is about 200 mV lower, a relative change of cell voltage of only 20−30%. For the conventional silicon cell the cell voltage decreases by a factor of 3 for a comparable change of light intensity showing that the photovoltage of our cells is significantly less sensitive to light intensity variations than in conventional photovoltaic devices. This is an important advantage for the application of the nanocrystalline cell in consumer electronic devices.

The overall efficiency (η_{global}) of the photovoltaic cell can easily be calculated from the integral photocurrent density (i_{ph}), the open circuit photovoltage (V_{oc}), the fill factor of the cell (ff) and the intensity of the incident light (I_s):

$$\eta_{global} = \frac{i_{ph} \times V_{oc} \times ff}{I_s} \qquad (23)$$

On the basis of $RuL_2(SCN)_2$ as sensitizer the photocurrent measured at 96.4 mW/cm^2 of simulated solar intensity (AM 1.5) was 18.3 mA/cm^2, the open circuit voltage was 0.72 V and the fill factor was 0.73 yielding for the overall efficiency of the cell a value of 10%.[101]

Contrary to chlorophyll in plants, which is renewed each springtime, a photosensitizer for solar cells also has to be stable for many years. Upon long illumination time, the $RuL_2(SCN)_2$ complex sustained more than 5×10^7 redox cycles without noticable loss of performance corresponding to ca. 10 years of continous operation in natural sunlight. By contrast, practically all organic sensitizers tested so far underwent photobleaching after less than 10^4 redox cycles. This clearly outlines the exceptionally stable operation of the newly developed ruthenium charge transfer sensitizers which is of great advantage for the practical application of these devices.

The energetics of all the three components in Figure 9 can be varied for optimal matching with regards to charge transfer. It should be noted that at least 100−200 mV is needed as driving force for the electron transfer reactions. Although we will primarily discuss the energetics of the nanocrystalline material in this paper, we note that large efforts are made to synthesize new dyes for better spectral overlap with the solar light[101,103] and to find an alternative to the I^-/I_3^- redox shuttle. As can be seen in Figure 9 about 0.4 V is actually lost in the reduction of the photoexcited dye by iodide, but so far no other candidates have been as efficient as the I^-/I_3^- couple when it comes to the kinetics of dye interception and electron uptake at the counter electrode.

The nanoporous TiO_2 electrode allows for potentiostatic control of the Fermi level and taking advantage of the transparency of the electrode it has been possible to spectroscopically monitor the accumulation of electrons within the conduction band and subsequent charge transfer processes at the interface.[136−138] The conduction band electrons create Ti^{3+} states, yielding a blue coloration of the film and the extinction coefficient at 780 nm is 3400 L mol^{-1} cm^{-1}.[138] The term "optical electrochemistry" has been coined from these investigations. Optical spectra of a 4 μm thick TiO_2 nanoporous film in a Li^+ containing acetonitrile electrolyte in the 400−800 nm wave-

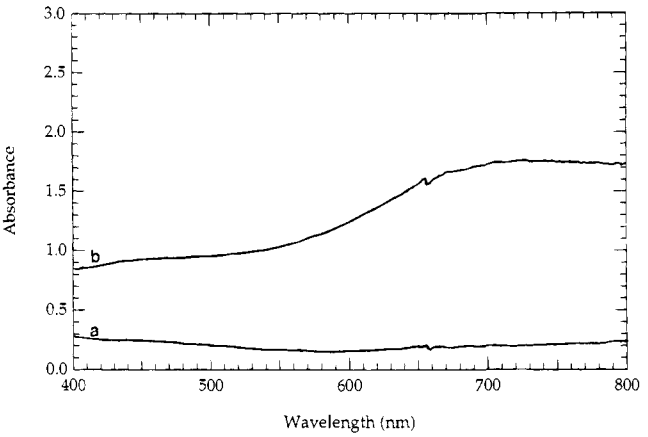

Figure 12. UV–vis spectral changes observed during electrochromic switching of nanocrystalline TiO_2 (a) bleached state (−0.64 V vs Ag/AgCl) and (b) colored state after polarizing to −1.64 V vs Ag/AgCl for 10 s. Electrolyte was 1 M $LiClO_4$ in acetonitrile; film thickness, 3.5 μm. The observed background absorption in the bleached state is due to light scattering. Ten seconds after applying the potential step the absorbance increases to a value above one in the whole visible region with a broad maximum of absorbance close to 2 in a wavelength interval of 660–800 nm. Charge passed is 0.10 C/cm^2.

length range at potentials positive respectively negative of the "flatband potential" are shown in Figure 12.

It should be noted that the term flatband potential is ill-defined for nanocrystalline electrodes. The term is appropriate for a compact semiconductor electrode forming a Schottky junction and a band bending in the depletion layer of the semiconductor. The flatband potential is then the potential where no electric field in the semiconductor exists, i.e. the bands are flat and the energy of the band edges can be estimated. As will be discussed below a space charge layer and a band bending is not likely to be formed in nanoporous semiconductor electrodes, except in the accumulation regime. A term like "the potential of the conduction band edge", V_{cb}, would therefore be better in nanocrystalline materials, and this terminology will be applied below.

If a potential of −0.64 V vs Ag/AgCl (saturated KCl in water) is applied to the nanocrystalline TiO_2 film in Figure 12, i.e. at a reverse bias, it shows essentially no coloration in the visible, curve a. The small attenuation of light observed here is due to light scattering and absorption by the two conducting glass sheets serving as outer confinements for the spectroelectrochemical cell. Changing the potential to −1.64 V in a stepwise fashion leads to intercalation of Li^+ and the appearance of an intensely dark blue coloration as shown by curve b in Figure 12. This absorption develops within a few seconds following the polarization step and disappears on the same time scale once the potential is switched back to the initial value. These are the underlying features of a present development in our laboratory, namely to utilize nanocrystalline TiO_2 electrodes for electrochromic devices.[111,112] A closer look at the absorbance spectrum in Figure 12 yields information concerning the nature of the electrons present in the conduction band. For free conduction band electrons, the extinction coefficient increases continuously with wavelength. The fact that the electron absorption has a maximum at 720 nm indicates that these charge carriers are trapped, which also has been discussed by O'Regan et al.[136] It was suggested, moreover, that the conduction band electrons are preferentially trapped at grain boundaries, expected to be present in a nanocrystalline film. By measuring the absorbance of the conduction band electrons as a function of applied potential it is therefore possible to obtain the potential of the conduction band edge as shown by Fitzmaurice and co-workers.[131,136–140] The pH dependence of V_{cb} for nanoporous TiO_2 films in aqueous solutions follows a Nernstian behavior with $V_{cb} = -0.40 - 0.06 \times \text{pH}$ (V/SCE).[138] Measurements in nonaqueous solutions have revealed that V_{cb} is directly related to the proton generating ability of the solvent.[140] A distinction between protic and aprotic solvents seems therefore to be more appropriate than aqueous and nonaqueous electrolyte.[140] In aprotic solvents V_{cb} may depend on the cation and Li^+, Na^+, and Mg^{2+} have been found to be potential determining ions.[140]

3.3. Observation and Importance of Electronic States in the Band Gap Region

Due to the high surface area of nanocrystalline electrodes the importance of surface states becomes very much pronounced in these systems compared to compact electrodes. By creating charge carriers in the nanoporous film, either by illumination or by a potentiostat, these charge carriers can be trapped in localized energy levels in the band gap region affecting the properties of the film. The observation and effect of trapped electrons in nanocrystalline semiconductor electrodes have been discussed in several papers.[54,101,109,112–114,130,132–134,136–139,141–145] Kay et al.[144] have interpreted cyclic voltammograms of nanocrystalline TiO_2 electrodes in terms of a tail of localized energy levels below the conduction band edge. The chemical nature of a localized energy level just below the conduction band edge is well established as a Ti^{3+} (3d) state.[146] The implication of electron trapping in the efficiency of the dye-sensitized solar cell can be multifold. Trapping of electrons in the bulk of the TiO_2 particle leads to a slow time response of the photocurrent but not to recombination losses. It will, however, lead to a lower position of the quasi-Fermi level for the electrons during illumination and thus to a reduced photovoltage. If electrons are trapped at the TiO_2 surface it may be a recombination pathway, i.e. it acts as an intermediate in the reduction of triiodide by conduction band electrons. This may lead to a lowering of the photocurrent, but also to a decrease in the photovoltage, which is due to a kinetic argument described by Lewis and co-workers.[147] For regenerative photoelectrochemical systems, the following relation holds:[147]

$$V_{oc} = \frac{kT}{e} \ln \frac{\eta_h \Phi_o}{n_{so} k_{ET}[OX]} \qquad (24)$$

where η_h is the quantum yield for photogenerated holes to reach the SEI, Φ_o the incident photon flux, n_{so} the equilibrium (dark) surface electron concentra-

tion, and k_{ET} the bimolecular rate constant for the forward (cathodic) electron transfer processes to the acceptor, OX, in the solution. Another argument put forward by Könenkamp et al.[113] is that electron trapping results in improvements in the photoresponse due to a change in the decay kinetics, i.e. the nanocrystalline TiO_2 electrode shows a photoconductive effect and therefore improved transport properties under trap-filled conditions.

From the above it follows that one of the key issues to improve the efficiencies of the dye-sensitized TiO_2 solar cell is to reduce the rate for triiodide reduction, i.e. to block the surface states below the conduction band edge. Since the photocurrent quantum yield is practically unity in the device[100,101] this will merely effect the values of the photovoltage. It has been shown[101] that treatment with 4-*tert*-butylpyridine on the TiO_2 surface increases the photovoltage by about 0.3 V, corresponding to a 5.5×10^4-fold decrease in the rate constant for triiodide reduction (eq 24). The importance of Ti^{3+} surface states in mediating interfacial charge transfer processes at the TiO_2–solution boundary has recently been established by laser photolysis studies[3] and by the optical electrochemical method.[143]

For nanoporous TiO_2 films the existence of extended states near the mid-band gap region has been suggested.[114] Some other evidence for states at about 1.4–1.5 eV below the conduction band edge,[148] discussed in terms of Ti–OH species, can be found in the literature. An energy level in the mid-band gap region would be a deep trap state for the charge carriers and the influence of deep traps in the dynamics of a dye-sensitized TiO_2 nanocrystalline electrode have been discussed[54,137,141] and simulated with a model calculation.[142]

3.4. Photoinduced Processes in Nanocrystalline Semiconductor Electrodes

The conductivity of nanophase TiO_2 films in vacuum have been found very low, $\sim 10^{-9}$ $(\Omega\ cm)^{-1}$ at room temperature.[54,113,114] However, under exposure to UV light the conductivity is strongly increased,[54,113,115] indicating that the low conductivity in dark is due to a low electron concentration in the conduction band rather than to poor electrical contact between the particles. The photoconductive effect has been interpreted by trap filling with recombination times considerably slower than the trapping processes under reverse bias.[113,114]

By immersing a semiconductor into an electrolyte the Fermi levels (usually called the electrochemical potential in the electrolyte) of the two phases are adjusted. For a compact semiconductor, e.g. a single crystal, a space charge layer will be formed, normally depicted as a band bending in energy level diagrams of the SEI (cf. ref 149). The charge separation process of the photoexcited electron–hole pair occurs then in the electric field in the space charge region. The formation of a space charge layer in a nanocrystalline semiconductor is, however, questionable due to the small particle size. The charge separation process in nanocrystalline electrodes was measured independently for colloidal TiO_2 films[107] and electrodeposited CdS and chemically deposited CdSe

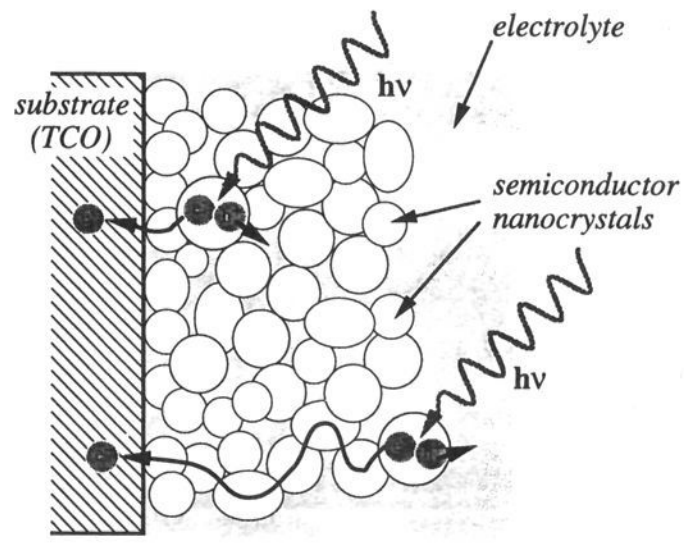

Figure 13. Model of the charge carrier separation and charge transport in a nanocrystalline film. The electrolyte has contact with the individual nanocrystallites. Illumination produces an electron–hole pair in one crystallite. The hole transfers to the electrolyte and the electron transverses several crystallites before reaching the substrate. Note that the photogenerated hole always has a short way (about the radius of the particle) to pass before reaching the semiconductor–electrolyte interface wherever the eletron–hole pair is created in the nanoporous film. The probability for the electron to recombine will, however, depend on the distance between the photoexcited particle and the TCO back-contact.

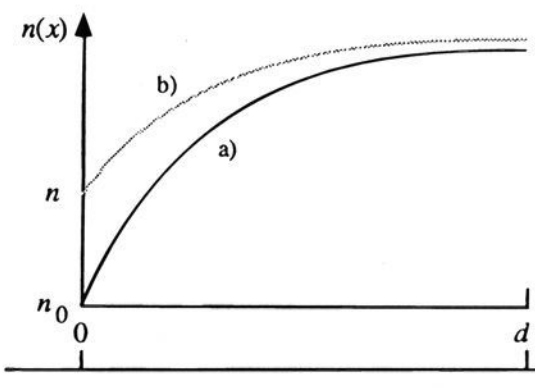

Figure 14. Electron concentration profile in a nanoporous semiconductor electrode during illumination. Curve a displays the electron concentration when the cell is unloaded (short circuit condition), whereas in curve b the cell is loaded. The semiconductor–TCO interface is placed at the position of the *y* axis.

films.[102] High quantum yields were measured in both cases. By illuminating the nanocrystalline film both through the electrolyte (front-side illumination) and through the TCO substrate (back-side illumination) the dependence of the quantum yield as a function of depth in the semiconductor film could be monitored.[102,107] From these measurements a qualitative model to describe the photocurrent generation in nanocrystalline films was presented, see Figure 13: The electrolyte penetrates the whole colloidal film up to the surface of the back contact and a semiconductor/electrolyte junction occurs thus at each nanocrystal, much like a normal colloidal system. During illumination, light absorption in any individual colloidal particle will generate an electron–hole pair. Assuming that the kinetics of charge transfer to the electrolyte is much faster for one of the charges (holes for TiO_2) than the recombination processes, the other charge (electrons) can create a gradient in the electrochemical potential between the particle and the back contact, see Figure 14. In this gradient the electrons (for TiO_2) can be transported through the interconnected colloidal particles to the back-contact, where they are withdrawn as a current. The charge

separation in a nanocrystalline semiconductor does therefore not depend on a built-in electric field, i.e. a Schottky barrier, but is mainly determined by kinetics at the SEI. The creation of the light-induced electrochemical potential for the electrons in TiO_2 also explains the bulding up of a photovoltage. On the basis of these observations for TiO_2 films and by assuming that the charge carriers in the semiconductor film are transported via diffusion and no mass transport limitations in the electrolyte, Södergren et al.[150] have presented a quantitative model to describe the photoelectrochemical properties of nanocrystalline electrodes. At present capacitance measurements and laser flash photolysis are carried out in our laboratory to follow the dynamics of the charge separation process and the charge transport in nanoporous TiO_2 electrodes. Parts of these investigations have been published in ref 151.

From the above discussion it is also clear that there will be an increased probability of recombination with increasing film thickness, as the electron has, on average, to be transported across an increasing number of colloidal particles and grain boundaries. This has also been observed experimentally.[102,107,125] Since the optical densities increase with increasing film thickness one can therefore conclude that there exists an optimal film thickness to obtain a maximum photocurrent.[102,107,134] Another loss mechanism due to increasing film thickness is a resistance loss leading to a decrease in photovoltage and fill factor. An important ingredient to obtain higher efficiencies with the dye-sensitized TiO_2 electrode is then to synthesize dyes with higher extinction coefficients in order to use thinner semiconductor films.

Interestingly, Hodes et al.[102] showed that depending on light etching treatments and the electrolyte (using effecient electron or hole acceptors), the photocurrent at the same electrode could switch direction, *behaving* as p- or n-doped semiconductors. In this regard, n-type behavior means preferential hole injection into the electrolyte while p-type behavior means preferential electron injection. Which behavior will occur depends then on the electrolyte and on the semiconductor surface. This is further evidence that charge separation in these systems does not occur by a space charge layer, which would not be expected to be affected by etching, in contrast to the nature of the surface of the nanocrystallites which would be affected. Later Kamat and co-workers confirmed the results of front-side/back-side illumination on e.g. coupled TiO_2/CdSe nanocrystalline films,[125] and the above-mentioned view of charge carrier separation in nanoporous electrodes as dominated by kinetics at the SEI seems to be generally accepted.

3.5 The Electric Field in a Nanocrystalline Electrode

Today, the definite answer to the question of the potential distribution in nanocrystalline electrodes is not known. However, some remarks on this issue have been made in the literature which we will discuss in the following. By applying an external bias O'Regan et al.[54] found that alterations of the electrode potential dramatically changed the interfacial charge transfer processes. In light of the above-mentioned results and discussion this may therefore be a bit surprising. So, how to understand the effect of an applied potential? A qualitative way of describing the effect of an external field on the charge transport in the semiconductor film can be made from Figure 14.[130,150] With increasing negative potential, the Fermi level at the back-contact/semiconductor interface will increase compared to zero bias and consequently the electron concentration will also increase from n_0 to n (see Figure 14). This causes a smaller gradient in the electrochemical potential of the electrons during illumination, resulting in less efficient charge transport. By increasing the negative potential further, the photocurrent decreases until it drops to zero when the photocurrent onset is reached. This potential is then the same as the photovoltage produced by the system. In this context we must also distinguish between two completely different cases, namely the situations under forward (accumulation mode) and reverse (depletion mode) bias. The variation of the potential with distance in bulk TiO_2 considered as isotropic) from the SEI corresponding to the edge of the conduction band has been calculated by Rothenberger et al.[138] In order to keep the calculations as simple as possible they considered a one-dimensional model of the SEI, i.e. a flat interface. By solving the Poisson's equation they found an asymmetry of the potential on both sides of the potential of the conduction band edge; the thickness of the space charge layer being much larger in a depletion mode than in an accumulation mode. For a 1 V potential difference between the bulk and the surface of the semiconductor, and by assuming a concentration of the conduction band electrons in the bulk to 10^{22} m^{-3}, the space charge layer in the depletion mode is about 1 μm thick, whereas in the accumulation mode it is about 5 nm thick. This means that the situation of the potential in the nanocrystalline electrode under forward bias can be discussed in terms of the formation of an accumulation layer created in each individual nanocrystal. The formation of a space charge layer under reverse bias is much more unclear and more experiments definitely need to be done to clarify this question. There are indications that the applied reverse potential is more effective for photocurrent yields on the layers close to the TCO contact than on the outer layers as measured by front-side/back-side illumination at different potentials on Fe_2O_3[133] and TiO_2[145] electrodes. We believe, however, that the most dominating effect of the applied reverse bias is the emptying and filling of trap states.[54]

On the basis of the discussions above we have drawn schematic energy level diagrams of the TCO/TiO_2/electrolyte system. It should be kept in mind that, since the colloidal TiO_2 film is porous to the TCO glass, the conducting glass substrate is also in contact with the electrolyte. In Figure 15a we show the situation under equilibrium in dark. Since the electrolyte penetrates the whole film up to the back contact, the band edge positions remain fixed through the whole TiO_2 film. The indications of the TiO_2 surface state levels are drawn through the whole colloidal film, since the SEI is accessible through the

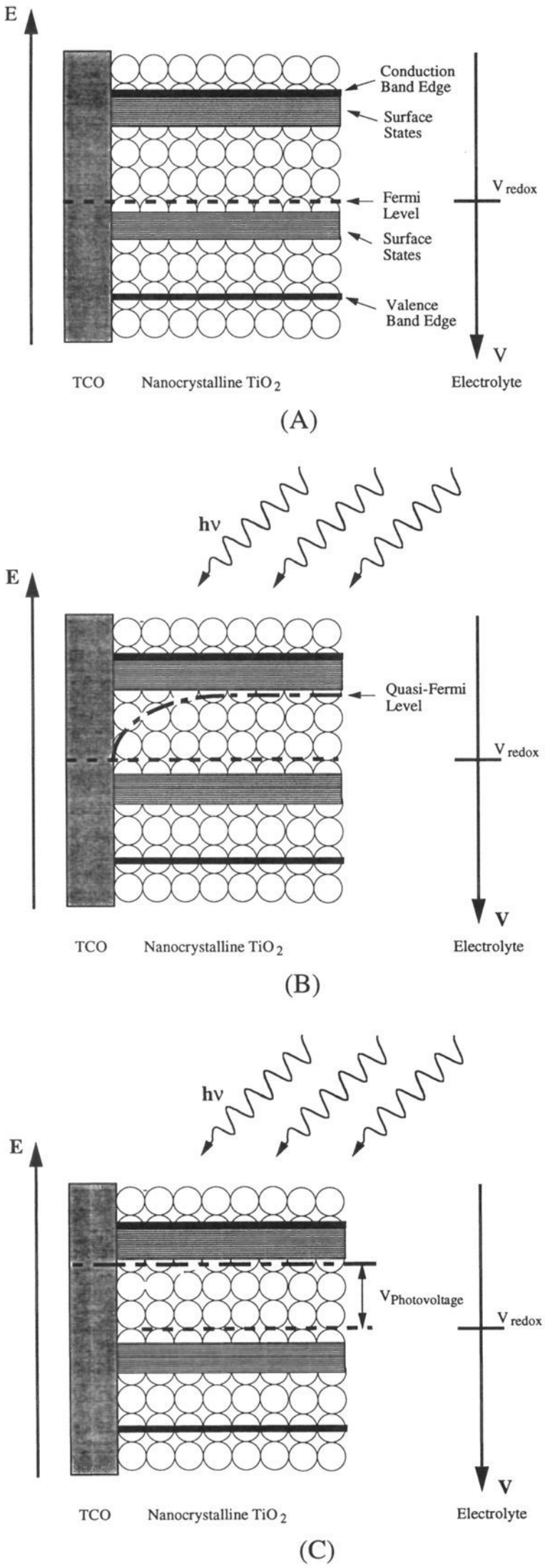

Figure 15. Schematic energy level diagrams of the TCO/TiO_2/electrolyte interface under different conditions: (a) in dark equilibrium, (b) illumination, short circuit, and (c) illumination, open circuit. V_{redox} = the redox potential of the electrolyte. See text for further details.

outmost layers of the film to the TCO glass. The system under illumination and short-circuit conditions can be seen in Figure 15b. The gradient in the electron concentration in the semiconductor from the outer layers to TCO contact is depicted by a bent quasi-Fermi level of the electrons and a current is drawn through the system (compare with Figure 14). As pointed out by Hoyer et al.[130] a gradient in the surface potential over the entire thickness of the film may be induced by a change of the pH value inside the pores because of redox reactions or an accumulation of cations near the back contact. Local pH changes in nanocrystalline TiO_2 film have been observed[137] in an aqueous electrolyte at pH = 3. A change of 2.5 pH units was calculated corresponding to a surface potential shift of 0.15 V. In an alkaline electrolyte, pH = 11.6, this effect was not observed and the effect is therefore relatively small and not included in our schematic energy level diagram. The open circuit condition and the buildup of a photovoltage is illustrated in Figure 15c. It can be noted here that a complex situation will occur at the back-contact where a contact point between all three phases, i.e. TCO, TiO_2, and electrolyte, can be envisaged.

3.6. Kinetic Rate Constants in the Photosensitized Solar Cell

That the charge separation mechanism is mainly governed by kinetics in nanocrystalline semiconductor electrodes and especially in the photosensitized photovoltaic cell is comparable to that of natural photosynthesis, where an electron is rapidly transferred from the excited reaction center chlorophyll to a distant acceptor of lower energy (the trap), thus preventing recombination before reduction of the chlorophyll cation by an electron donor has taken place. Today no complete picture of the kinetics for a given Ru complex photosensitized TiO_2 photovoltaic cell can be drawn. But on the basis of different measurements it is possible to indicate the orders of magnitude for the rate constants of the reaction steps in the solar cell, see Figure 16. Following light absorption of the Ru dye (1), the electron injection into the conduction band (2) is in the picosecond range. Eichberger and Willig[152] showed that the electron injection from a *cis*-diaquabis(2,2′-bipyridyl-4,4′-dicarboxylate)ruthenium(II) adsorbed on TiO_2 was ultrafast (τ < 7 ps) with a quantum yield near 100%. As discussed in sections 2.4.3 and 3.2 the rate of the back-reaction (3) is much smaller, typically $\tau \approx 1\ \mu$s. Another important recombination process in the cell is the reduction of triiodide in the electrolyte by conduction band electrons (4). The exchange current density, j_o, or the reverse saturation current, of this process has been measured by Smestad.[153] Values between 10^{-11}–10^{-9} A/cm^2 were obtained depending on the electrolyte. From section 3.3 we know also that these values can be drastically changed by surface treatments. The electron movement in the nanocrystalline TiO_2 electrode to the back-contact (5) is significantly slower than in single-crystal TiO_2. Measurements in our laboratory[151] have shown that the photocurrent transients, following UV excitation of the TiO_2 particles from a nanosecond pulse laser, decay in the millisecond to second range. The exchange current density, j_o, for reduction of triiodide at the counter electrode (TCO glass coated with a catalytic amount of platinum) (6),

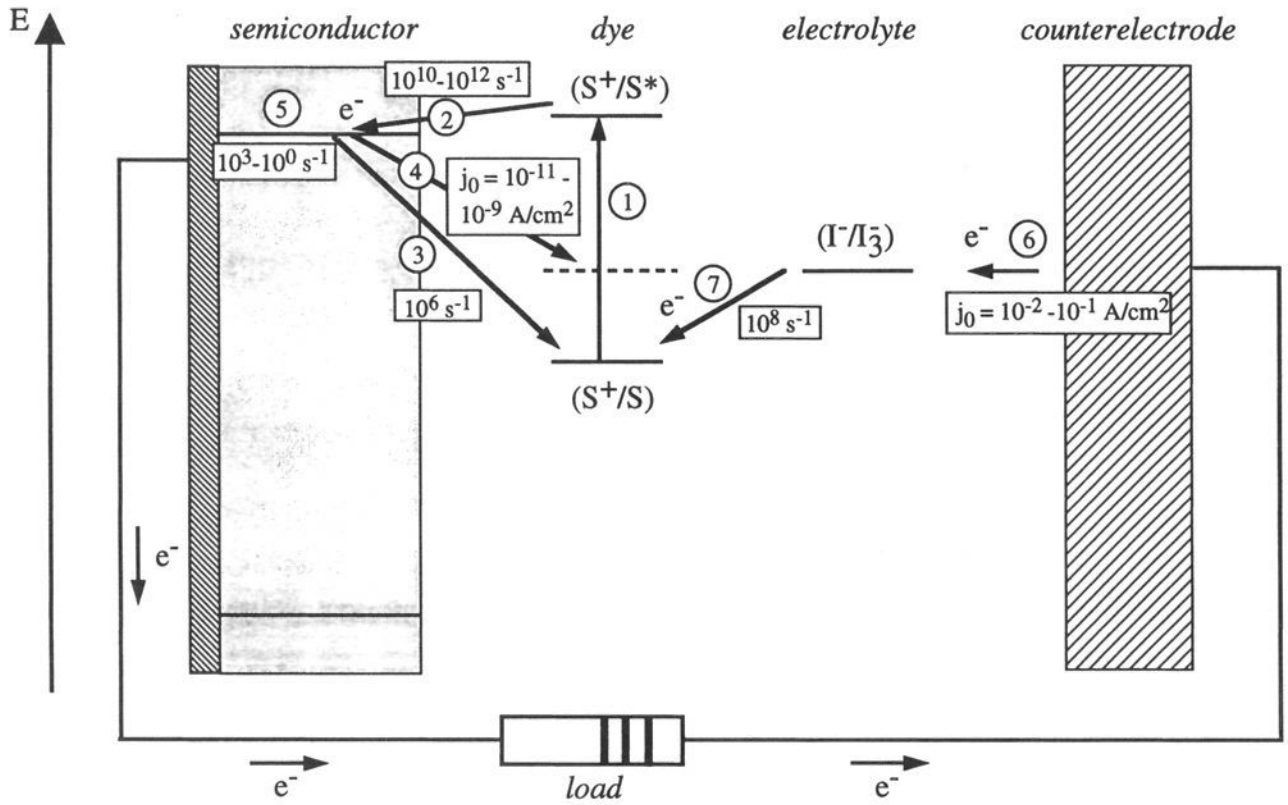

Figure 16. Scheme summarizing the characteristic rate constants for the important reaction steps associated with electron–hole pair separation and recombination in Ru complex photosensitized nanocrystalline TiO_2 electrodes. Details are explained in the text.

has been measured to $(10^{-2}–2) \times 10^{-1}$ A/cm^2.[154] Finally, the reduction of the oxidized dye by iodide (7) occurs on a time scale of 10^{-8} s.[101]

For the photosensitizaion of TiO_2 solar cells, Ru–bipyridine complexes have proven to be currently the most efficient, due to their broad absorption spectra combined with favorable photoelectrochemical properties and high stability in the oxidized state.[101] However, with interest to artificial photosynthetic systems the TiO_2 colloidal film electrode has been sensitized with derivatives of chlorophyll and related natural porphyrins resulting in light harvesting and charge separation efficiencies comparable to those in natural photosynthesis.[144,155,156] For example an energy conversion efficiency of 10% for TiO_2 solar cells sensitized with copper chlorophyllin was obtained at the red peak at 630 nm.[155] The overall energy conversion efficiency of this cell was 2.6% under simulated sunlight illumination.

In conclusion the high efficiencies and high stability of the dye-sensitized nanocrystalline TiO_2 solar cell can be explained by favorable kinetics for the desired pathway of the photoexcited electron. The charge transport through the colloidal TiO_2 film is probably also improved by trap filling in the semiconductor material, in other words the solar cell shows a photoconductive effect. The major advantages of the solar cell as we see it today is the possibility of making semitransparent photovoltaic devices and the economical aspects.[106] The cell is prepared from low to medium purity materials through low-cost processes. Apart from efficiency and stability any future photovoltaic technology will be valued according to its environmental and human compatibility. There is great concern about the adverse environmental effects and acute toxicity of CdTe or $CuInSe_2$ which are being considered for practical development as thin solar cells. Such concerns are unjustified for our nanocrystalline device. TiO_2 is a harmless environment-friendly material, remarkable for its very high stability. It occurs in nature as ilmenite, and is e.g. used in quantity as a white pigment and as an additive in toothpaste. Similarly ruthenium has been used without adverse health effects as an additive for bone implants. We also believe that nanocrystalline electrodes with a very high effective surface area and the possibility to prepare them with different optical characteristics will find more applications and use in fundamental research.

From a fundamental point of view further investigations of the kinetics, especially in a two-electrode system, at the SEI are needed. The energetics and chemical nature of energy levels in the band gap region, trap states, must be further elucidated. The detailed mechanism of the charge transport through the colloidal particles is not known. A hopping type mechanism has been suggested[113,144] and the possibility of tunneling through a potential barrier between the particles has been mentioned.[130] As discussed in section 3.5 the potential distribution in nanocrystalline semiconductor electrodes remains uncertain.

4. Acknowledgements

This work was supported by the Swiss National Science Foundation.

5. References

(1) *Photoinduced Electron Transfer*; Fox, M. A., Chanon, M., Eds.; Elsevier; Amsterdam, 1988.
(2) Wang, C.; Heller, A.; Gerischer, H. *J. Am. Chem. Soc.* **1992**, *114*, 5230.
(3) Moser, J.; Punichihewa, S.; Infelta, P. P.; Grätzel, M. *Langmuir* **1991**, *7*, 3012.
(4) McEvoy, A. J.; Grätzel, M. *Sol. Energy Mater. Sol. Cells* **1994**, *32*, 221.
(5) Grätzel, M. *Acc. Chem. Res.* **1981**, *14*, 376.
(6) Duonghong, D.; Borgarello, E.; Grätzel, M. *J. Am. Chem. Soc.* **1981**, *103*, 4685.
(7) Kiwi, J. *Chem. Phys. Lett.* **1981**, *83*, 593.
(8) Brus, L. E. *J. Phys. Chem.* **1986**, *90*, 2555.
(9) Matijevic, E. *Langmuir* **1986**, *2*, 12.
(10) Fendler, J. H. *Chem. Rev.* **1987**, *87*, 877.

(11) Henglein, A. *Top. Curr. Chem.* **1988**, 143.
(12) Henglein, A. *Chem. Rev.* **1989**, *89*, 1861.
(13) Kamat, P. V.; Dimitrijevic. *Sol. Energy*, **1990**, *44*, 83.
(14) Turchi, C. S.; Ollis, D. F. *J. Catal.* **1990**, *122*, 178.
(15) Fox, M. A. *Res. Chem. Intermed.* **1991**, *15*, 153.
(16) Ollis, D.; Pelizzetti, E.; Serpone, N. *Environ. Sci. Technol.* **1991**, *25*, 1522.
(17) Kamat, P. V. *Chem. Rev.* **1993**, *93*, 267.
(18) Ollis, D.; El-Akabi, H. *TiO_2 Photocatalytic Purification and Treatment of Water and Air*; Elsevier: New York, 1993.
(19) Moser, J.; Grätzel, M. *Helv. Chim. Acta* **1982**, *65*, 1436.
(20) Koch, U.; Foitik, A.; Weller, H.; Henglein, A. *Chem. Phys. Lett.* **1985**, *122*, 507.
(21) Micic, O. I. Private communication.
(22) Naman, S. A.; Aliwi, S. M.; Al-Emaru, K. *Nouv. J. Chim.* **1985**, *9*, 687.
(23) Mann, S.; Williams, R. J. P. *J. Chem. Soc., Dalton Trans.* **1983**, 331.
(24) Parmon, V. Plenary lecture VIIth International Conference on Solar Energy Conversion, Chicago, IL, 1988.
(25) Rossetti, R.; Beck, S. M.; Brus, L. *J. Am. Chem. Soc.* **1984**, *106*, 980.
(26) Micic, O. I.; Nenadovic, M. T.; Peterson, M. W.; Nozik, A. J. *J. Phys. Chem.* **1987**, *91*, 1295.
(27) Sandroff, C. J.; Kelty, S. P.; Hwang, D. M. *J. Chem. Phys.* **1986**, *85*, 5373.
(28) Peterson, M. W.; Nenadovic, M. T.; Rajh, T.; Herak, R.; Micic, O. I.; Goral, J. P.; Nozik, A. J. *J. Phys. Chem.* **1988**, *22*, 1400.
(29) Sandroff, C. J.; Chung, M. *J. Colloid Interface Sci.* **1987**, *115*, 593.
(30) Foitik, A.; Weller, H.; Henglein, A. *Chem. Phys. Lett.* **1985**, *120*, 552.
(31) Micic, O. I.; Zongguan, L.; Mills, G.; Sullivand, J. C.; Meisel, D. *J. Phys. Chem.* **1987**, *91*, 6221.
(32) Berry, C. R. *Phys. Rev.* **1967**, *161*, 848.
(33) (a) Brus, L. E. *J. Phys. Chem.* **1986**, *90*, 2555 and references therein. (b) Brus, L. E. *J. Chem. Phys.* **1984**, *80*, 4403. (c) Rossetti, R.; Hull, R.; Gibson, J. M.; Brus, L. E. *J. Chem. Phys.* **1985**, *83*, 1406.
(34) (a) Weller, H.; Schmidt, H. M.; Koch, U.; Fojtik, A.; Baral, S.; Henglein, A.; Kunath, W.; Weiss, K.; Dieman, E. *Chem. Phys. Lett.* **1984**, *124*, 557 and references therein. (b) Weller, H.; Koch, U.; Gutierrez, M.; Henglein, A. *Ber. Bunsen-Ges. Phys. Chem.* **1984**, *88*, 649.
(35) Nozik, A. J.; Williams, F.; Nenadovic, M. T.; Rajh, T.; Micic, O. I. *J. Phys. Chem.* **1985**, *89*, 397. (b) Nedeljkovic, J. M.; Nenadovic, M. T.; Micic, O. I.; Nozik, A. J. *J. Phys. Chem.* **1986**, *90*, 12.
(36) Ramsden, J. J.; Webber, S. E.; Grätzel, M. *J. Phys. Chem.* **1985**, *89*, 2740.
(37) Tricot, Y.-M.; Fendler, J. H. *J. Phys. Chem.* **1986**, *90*, 3369.
(38) Variano, B. F.; Hwang, D. M.; Sandroff, C. J.; Wiltzins, P.; Jing, T. W.; Ong, N. P. *J. Phys. Chem.* **1987**, *91*, 6455.
(39) Dannhauser, T.; O'Neill, M.; Johansson, K.; Whitten, D.; McLendon, G. *J. Phys. Chem.* **1986**, *90*, 6074.
(40) (a) Ekimov, A. I.; Onushchenko, A. A. *JETP Lett.* **1984**, *40*, 1136. (b) Ekimov, A. I.; Efros, Al. L.; Onushchenko, A. A. *Solid State Commun.* **1985**, *56*, 921. (c) Efros, Al. L.; Efros, A. L. *Sov. Phys.-Semicond. (Engl. Transl.)* **1982**, *16*, 772.
(41) Borrelli, N. F.; Hall, D. W.; Holland, H. J.; Smith, D. W. *J. Appl. Phys.* **1987**, *61*, 5399.
(42) Wang, Y.; Mahler, W. *Opt. Commun.* **1987**, *61*, 233.
(43) Wang, Y.; Suna, A.; Mahler, W.; Kasowsi, R. *J. Chem. Phys.* **1987**, *87*, 7315.
(44) Wang, Y.; Herron, N. *J. Phys. Chem.* **1987**, *91*, 5005.
(45) Kakuta, N.; White, J. M.; Campion, A.; Fox, M. A.; Webber, S. E. *J. Phys. Chem.* **1985**, *89*, 48.
(46) Wang, Y.; Herron, N. *J. Phys. Chem.* **1988**, *92*, 4988.
(47) Herron, N.; Wang, Y.; Eddy, M.; Stucky, G.; Cox, D. E.; Bein, T. *J. Am. Chem. Soc.* **1989**, *111*, 530.
(48) Tricot, Y. M.; Fendler, J. H. In *Homogeneous and Heterogeneous Photocatalysis*; Pelizzetti, E., Serpone, N., Eds.; NATO ASI Series C; D. Reidel: Dordrecht, 1986; Vol. 174, pp 241ff.
(49) Fendler, J. H. *J. Phys. Chem.* **1985**, *89*, 2730.
(50) Steigerwald, M. C.; et al. *J. Am. Chem. Soc.* **1988**, *110*, 3046.
(51) Zhao, X. K.; Baral, S.; Rolandi, R.; Fendler, J. H. *J. Am. Chem. Soc.* **1988**, *119*, 1012.
(52) Thurner, J. E.; Henderwerk, M.; Parmeter, J.; Somorjai, G. A. *J. Electrochem. Soc.* **1984**, *131*, 1777.
(53) Anderson, M. A.; Geiselmann, M. J.; Xu, J. Q. *J. Membr. Sci.* **1988**, *39*, 243.
(54) O'Regan, B.; Moser, J.; Anderson, M.; Grätzel, M. *J. Phys. Chem.* **1990**, *94*, 8720.
(55) Grätzel, M. *Heterogeneous Photochemical Electron Transfer*; CRC Press: Baton Rouge, FL, 1988.
(56) Dutton, D. *Phys. Rev.* **1985**, *112*, 785.
(57) (a) Ramsden, J. J.; Grätzel, M. *J. Chem. Soc., Faraday Trans. 1* **1984**, *80*, 919. (b) Ramsden, J. J.; Webber, S. E.; Grätzel, M. *J. Phys. Chem.* **1985**, *89*, 2740.
(58) Kreibich, U.; Fragstein, C. *Z. Phys.* **1969**, *224*, 307.
(59) Papavassiliou, G. C. *Prog. Solid State Chem.* **1979**, *12*, 185.
(60) Hsu, W. P.; Matijevic, E. *Appl. Opt.* **1985**, *24*, 1623.
(61) Fröhlich, H. *Physica* **1937**, *6*, 406.
(62) Kubo, R.; Kawabata, A.; Kabayashi, S. *Annu. Rev. Mater. Sci.* **1984**, *14*, 49.
(63) (a) Chang, L. L.; Esaki, L.; Howard, W. E.; Ludeke, R. *J. Vac. Sci. Technol.* **1973**, *10*, 11. (b) Cho, A. Y.; Arthur, J. R. *Prog. Solid State Chem.* **1975**, *10*, 157; (c) Dingle, R.; Gossard, A. C.; Wiegmann, W. *Phys. Rev. Lett.* **1975**, *34*, 1327.
(64) Chemla, D. S.; Miller, D. A. B. *J. Opt. Soc. Am. B: Opt. Phys.* **1985**, *2*, 1155.
(65) Taeckel, G. v. *Z. Tech. Phys.* **1926**, *7*, 301.
(66) Inmau, J. K.; Mraz, A. M.; Weyl, W. A. *Solid Luminescent Materials*; Wiley: New York, pp 182, 1948.
(67) Berry, C. R. *Phys. Rev.* **1967**, *161*, 848.
(68) Hayashi, S.; Nakamori, N.; Kanamori, H.; Yodogawa, Y.; Yamamoto, K. *Surface Sci.* **1979**, *86*, 665.
(69) Stasenko, A. G. *Sov. Phys. Solid State* **1968**, *10*, 186.
(70) Skomyakov, L. G.; Kitaev, G. A.; Shcherbakova, Ya.; Belyaeva, N. N. *Opt. Spectrosc.* **1978**, *44*, 82.
(71) Nedeljkovic, J. M.; Nenadovic, M. T.; Micic, O. I.; Nozik, A. J. *J. Phys. Chem.* **1986**, *90*, 12.
(72) Weller, H.; Foitik, A.; Henglein, A. *Chem. Phys. Lett.* **1985**, *117*, 485.
(73) Brus, L. E. *J. Chem. Phys.* **1984**, *80*; 4403; **1983**, *79*, 5566.
(74) Bawendi, M. G.; Steigerwald, M. L.; Brus, L. E. *Annu. Rev. Phys. Chem.* **1990**, *41*, 477.
(75) Weller, H.; Schmidt, H. M.; Koch, U.; Foitik, A.; Baral, S.; Henglein, A.; Kunath, W.; Weiss, K.; Diekmann, E. *Chem. Phys. Lett.* **1986**, *124*, 557.
(76) Serpone, N.; Sharma, D. K.; Jamieson, M. A.; Grätzel, M.; Ramsden, J. J. *Chem. Phys. Lett.* **1985**, *115*, 473.
(77) Nosaka, Y.; Fox, M. A. *J. Phys. Chem.* **1988**, *92*, 1892.
(78) Thomas, J. K. *J. Phys. Chem.* **1987**, *91*, 207.
(79) Albery, W. J.; Bartlett, P. N. *J. Electrochem. Soc.* **1984**, *131*, 315.
(80) Curran, J. S.; Lamouche, D. *J. Phys. Chem.* **1983**, *87*, 5405.
(81) Duonghong, D.; Ramsden, J. J.; Grätzel, M. *J. Am. Chem. Soc.* **1982**, *104*, 2977.
(82) Moser, J.; Grätzel, M. *J. Am. Chem. Soc.* **1983**, *105*, 6547.
(83) Kuczynski, J.; Thomas, J. K. *Chem. Phys. Lett.* **1982**, *88*, 4445.
(84) Grätzel, M. *Acc. Chem. Res.* **1981**, *14*, 376.
(85) Brown, G. T.; Darwent, J. R. *J. Chem. Soc. Chem. Commun.* **1985** 93.
(86) Mulvaney, P.; Swayambunathan, V.; Grieser, F.; Meisel, D. *J. Phys. Chem.* **1988**, *92*, 6732.
(87) Lewis, N. *Annu. Rev. Phys. Chem.* **1991**, *42*, 543.
(88) Albery, W. J. *J. Am. Chem. Soc.* **1985**, *107*, 1854.
(89) Bourdon, J. *J. Phys. Chem.* **1965**, *69*, 705.
(90) Borg, W. E.; Hauffe, K. H. *Current Problems in Electrophotography*; de Gruyter: Berlin, 1972.
(91) (a) Giraudeau, A.; Fan, F. R. F.; Bard, A. J. *J. Am. Chem. Soc.* **1980**, *102*, 5137 and references therein. (b) Gosh, P. K.; Spiro, T. G. *J. Am. Chem. Soc.* **1980**, *102*, 5543. (c) Dave-Edwards, M. P.; Goodenough, J. B.; Hamnet, A. J.; Seddon, K. R.; Wright, R. D. *Faraday Discuss. Chem. Soc.* **1980**, *70*, 285. (d) Mackor, A.; Schoonman, J. *Recl. Trav. Chim. Pays-Bas* **1980**, *99*, 71. (d) Memming, R. *Surf. Sci.* **1980**, *101*, 551.
(92) (a) Clark, W. D. K.; Sutin, D. *J. Am. Chem. Soc.* **1977**, *99*, 4676. (b) Tinnemans, A. H. A.; Mackor, A. *Recl. Trav. Chim. Pays-Bas*, **1981**, *100*, 295. (c) Hamnet, A. J.; Dave-Edwards, M. P.; Wright, R. D.; Seddon, K. R.; Goodenough, J. B. *J. Phys. Chem.* **1979**, *83*, 3280.
(93) Gleria, M.; Memming, R. *Z. Phys. Chem., N.F.* **1975**, *98*, 303.
(94) Matsumura, M.; Mitsuda, K.; Yoshizawa, N.; Tsubomura, H. *Bull. Chem. Soc. Jpn.* **1981**, *54*, 692.
(95) Enea, O.; Moser, J.; Grätzel, M. *J. Electroanal. Chem.* **1989**, *259*, 59.
(96) Moser, J.; Grätzel, M. *Chem. Phys.* **1993**, *176*, 493.
(97) Kalyanasundaram, K.; Vlachopoulos, N.; Krishnan, V.; Monnier, A.; Grätzel, M. *J. Phys. Chem.* **1987**, *91*, 2342.
(98) (a) Desilvestro, J.; Grätzel, M.; Kavan, L.; Moser, J.; Augustynski, J. *J. Am. Chem. Soc.* **1985**, *107*, 2988. (b) Vlachopoulos, N.; Liska, P.; Augustynski, J.; Grätzel, M. *J. Am. Chem. Soc.* **1988**, *110*, 1216.
(99) Vrachnou, E.; Vlachopoulos, N.; Grätzel, M. *J. Chem. Soc. Chem. Commun.* **1987**, 868.
(100) O'Regan, B.; Grätzel, M. *Nature* **1991**, *353*, 737.
(101) Nazeruddin, M. K.; Kay, A.; Rodicio, I.; Humphry-Baker, R.; Müller, E.; Liska, P.; Vlachopoulos, N.; Grätzel, M. *J. Am. Chem. Soc.* **1993**, *115*, 6382.
(102) Hodes, G.; Howell, I. D. J.; Peter, L. M. *J. Electrochem. Soc.* **1992**, *139*, 3136.
(103) Heimer, T. A.; Bignozzi, C. A.; Meyer, G. J. *J. Phys. Chem.* **1993**, *97*, 11987.
(104) Knoedler, R.; Sopka, J.; Harbach, F.; Guenling, H. W. *Sol. Energy Mat. Sol. Cells* **1993**, *30*, 277.
(105) Hagfeldt, A.; Didriksson, B.; Palmqvist, T.; Lindström, H.; Södergren, S.; Rensmo, H.; Lindquist, S.-E. *Sol. Energy Mat. Sol. Cells* **1994**, *31*, 481.

(106) Smestad, G.; Bignozzi, C.; Argazzi, R. *Sol. Energy Mat. Sol. Cells* **1994**, *32*, 259.
(107) Hagfeldt, A.; Björkstén, U.; Lindquist, S.-E. *Sol. Energy Mat. Sol. Cells* **1992**, *27*, 293.
(108) Meyer, G. J.; Searson, P. C. *Electrochem. Soc. Interface* **1993**, *2*, 23.
(109) Hotchandani, S.; Bedja, I.; Fessenden, R. W.; Kamat, P. V. *Langmuir* **1994**, *10*, 17.
(110) Marguerettaz, X.; O'Neill, R.; Fitzmaurize, D. *J. Am. Chem. Soc.* **1994**, *116*, 5017.
(111) Hagfeldt, A.; Vlachopoulos, N.; Grätzel, M. *J. Electrochem. Soc.* **1994**, *141*, L82.
(112) Hagfeldt, A.; Vlachopoulos, N.; Gilbert, S.; Grätzel, M. *Proc. SPIE-Int. Soc. Opt. Eng.*, in press (Optical Materials Technology for Energy Efficiency and Solar Energy Conversion XIII).
(113) Könenkamp, R.; Henninger, R.; Hoyer, P. *J. Phys. Chem.* **1993**, *97*, 7328.
(114) Könenkamp, R.; Henninger, R. *Appl. Phys. A* **1994**, *58*, 87.
(115) Hagfeldt, A.; Vlachopoulos, N.; Rothenberger, G.; Grätzel, M. *Book of Abstracts*; Tenth International Conference on Photochemical Conversion and Storage of Solar Energy, IPS-10, July 24–29, 1994, Interlaken, Switzerland; pp 207–208.
(116) Vinodgopal, K.; Hotchandani, S.; Kamat, P. V. *J. Phys. Chem.* **1993**, *97*, 9040.
(117) Grätzel, M.; Hagfeldt, A.; Mayor, M.; Walder, L. *Book of Abstracts*; Tenth International Conference on Photochemical Conversion and Storage of Solar Energy, IPS-10, July 24–29, 1994, Interlaken, Switzerland; p 159.
(118) Matthews, R. W. *J. Phys. Chem.* **1987**, *91*, 3328.
(119) Sabate, J.; Anderson, M. A.; Kikkawa, H.; Edwards, M.; Hill, C. G. *J. Catal.* **1991**, *127*, 167.
(120) Al-Ekabi, H.; Safarzadeh-Amiri, A.; Sifton, W.; Story, J. *Int. J. Environ. Pollut.* **1991**, *1*, 125.
(121) See ref 116.
(122) Vinodgopal, K.; Stafford, U.; Gray, K. A.; Kamat, P. V. *J. Phys. Chem.* **1994**, *98*, 6797.
(123) Kim, D. H.; Anderson, M. A. *Environ. Sci. Technol.* **1994**, *28*, 479.
(124) Vogel, R.; Pohl, K.; Weller, H. *Chem. Phys. Lett.* **1990**, *174*, 241.
(125) Vogel, R.; Hoyer, P.; Weller, H. *J. Phys. Chem.* **1994**, *98*, 3183.
(126) Liu, D.; Kamat, P. V. *J. Electroanal. Chem.* **1993**, *347*, 451.
(127) Liu, D.; Kamat, P. V. *J. Phys. Chem.* **1993**, *97*, 10769.
(128) Ennaoui, A.; Fiechter, S.; Tributsch, H.; Giersig, M.; Vogel, R.; Weller, H. *J. Electrochem. Soc.* **1992**, *139*, 2514.
(129) Sakohara, S.; Tickanen, L. D.; Anderson, M. A. *J. Phys. Chem.* **1992**, *96*, 11086.
(130) Hoyer, P.; Eichberger, R.; Weller, H. *Ber. Bunsen-Ges Phys. Chem.* **1993**, *97*, 630.
(131) Redmond, G.; O'Keefe, A.; Burgess, C.; MacHale, C.; Fitzmaurice, D. *J. Phys. Chem.* **1993**, *97*, 11081.
(132) Spanhel, L.; Anderson, M. A. *J. Am. Chem. Soc.* **1990**, *112*, 2278.
(133) Björkstén, U.; Moser, J.; Grätzel, M. *Chem. Mater.* **1994**, *6*, 858.
(134) Bedja, I.; Hotchandani, S.; Kamat, P. V. *J. Phys. Chem.*, in press. (We thank Dr. Kamat for sending us this information prior to publication.)
(135) Björkstén, U.; Shklover, V.; Grätzel, M. Manuscript in preparation.
(136) O'Regan, B.; Grätzel, M.; Fitzmaurice, D. *Chem. Phys. Lett.* **1991**, *183*, 89.
(137) O'Regan, B.; Grätzel, M.; Fitzmaurice, D. *J. Phys. Chem.* **1991**, *95*, 10525.
(138) Rothenberger, G.; Fitzmaurice, D.; Grätzel, M. *J. Phys. Chem.* **1992**, *96*, 5983.
(139) Fitzmaurice, D. *Sol. Energy Mater. Sol. Cells* **1994**, *32*, 289.
(140) Redmond, G.; Fitzmaurice, D. *J. Phys. Chem.* **1993**, *97*, 1426.
(141) Willig, F.; Kietzmann, R.; Schwarzburg, K. In *Proceedings of the Ninth International Conference on Photochemical Conversion and Storage of Solar Energy*; IPS-9, August 23–28, 1992, Beijing, China; International Academic Publishers: Beijing China, 1992; pp 129–139 (ISBN 7-80003-254-3).
(142) Schwarzburg, K.; Willig, F. *Appl. Phys. Lett.* **1991**, **58**, 2520.
(143) Redmond, G.; Fitzmaurice, D.; Grätzel, M. *J. Phys. Chem.* **1993**, *97*, 6951.
(144) Kay, A.; Humphry-Baker, R.; Grätzel, M. *J. Phys. Chem.* **1994**, *98*, 952.
(145) Hagfeldt, A.; Lindquist, S.-E.; Grätzel, M. *Sol. Energy Mater. Sol. Cells* **1994**, *32*, 245.
(146) Cf. (a) Howe, R. F.; Grätzel, M. *J. Phys. Chem.* **1985**, *89*, 4495. (b) Göpel, W.; Anderson, J. A.; Frankel, D.; Jaehnig, M.; Phillips, K.; Schäfer, J. A.; Rocker, G. *Surf. Sci.* **1984**, *139*, 333.
(147) Kumar, A.; Santangelo, P. G.; Lewis, N. S. *J. Phys. Chem.* **1992**, *96*, 835.
(148) Cf. (a) Nakato, Y.; Tsumura, A.; Tsubomura, H. *J. Phys. Chem.* **1983**, *87*, 2402. (b) Sakamaki, K.; Itoh, K.; Fujishima, A.; Gohshi, Y. *J. Vac. Sci. Technol.* **1990**, *A8*, 614. (c) Lawless, D.; Serpone, N.; Meisel, D. *J. Phys. Chem.* **1991**, *95*, 5166. (d) Hagfeldt, A.; Lunell, S.; Siegbahn, H. O. G. *Int. J. Quantum Chem.* **1994**, *49*, 97.
(149) Koval, C. A.; Howard, J. N. *Chem. Rev.* **1992**, *92*, 411.
(150) Södergren, S.; Hagfeldt, A.; Olsson, J.; Lindquist, S.-E. *J. Phys. Chem.* **1994**, *98*, 5552.
(151) Björkstén, U.; Hagfeldt, A.; Moser, J.; Grätzel, M. *Book of Abstracts*; Tenth International Conference on Photochemical Conversion and Storage of Solar Energy, IPS-10, July 24–29, 1994, Interlaken, Switzerland; pp 209–210.
(152) Eichberger, R.; Willig, F. *Chem. Phys.* **1990**, *141*, 159.
(153) Smestad, G. *Sol. Energy Mater. Solar Cells* **1994**, *32*, 273.
(154) Papas, N.; Grätzel, M. Manuscript in preparation.
(155) Kay, A.; Grätzel, M. *J. Phys. Chem.* **1993**, *97*, 6272.
(156) Bedja, I.; Carpentier, R.; Hotchandani, S.; Fessenden, R. W.; Kamat, P. V. *J. Appl. Phys.*, submitted for publication. (We thank Dr. Kamat for sending us this information prior to publication.)

CR940118W